8. PRE-NECTARIAN SYSTEM

FIGURE 8.1 (OVERLEAF). —Predominantly pre-Nectarian terrane on northern farside, including densely cratered tracts and smoother areas covered by basin deposits and secondary craters. Orbiter 5 frame M–53.

8. PRE-NECTARIAN SYSTEM

CONTENTS

INTRODUCTION

The lunar pre-Nectarian system[8.1] provides our clearest look at the early Solar System. The barrage of cosmic bodies that must have affected all moons and planets is richly recorded by pre-Nectarian basins and large craters, which are packed more densely than those of any other age (pl. 6; fig. 8.1). Their deposits cover a triangular area of the southern nearside and large parts of the farside. Smaller craters presumably formed in proportional abundance but were degraded by other craters (see chap. 7). Fine distinctions among facies of basin and crater deposits, which are observed in rayed craters and the Orientale basin, have similarly been blurred but can commonly be detected by comparisons with the younger analogs. Any maria that may have formed must have been even more completely devastated by the rain of impacts. Faults and folds dating from the pre-Nectarian are unknown, although they may have formed then as they did later. Therefore, efforts to understand early lunar and Solar-System history depend largely on interpreting the generally subdued and modified deposits of pre-Nectarian basins and craters.

Another look into the distant past is provided by the samples returned by the Apollo and Luna spacecraft (pl. 3). When fully evaluated, data from the sample analyses should show much about the composition of Solar-System material, the bulk composition of the Moon, and the processes by which a body of the Moon's size and composition differentiates. A major problem confronting analysts is distinguishing the effects of these early chemical and petrologic processes from those of the later impacts which formed the deposits that contain the samples. By definition, all materials formed since the origin of the Moon until the formation of the Nectaris basin are pre-Nectarian (Stuart-Alexander and Wilhelms, 1975). Accordingly, both the stratigraphic units that are still visible and the plutonic rocks of the early terra crust that were originally created by igneous processes are pre-Nectarian.

It is important to stress this distinction between the internal origin and impact emplacement of lunar terra rocks. The various groups of scientists that have investigated these two phases in the rocks' history have not always communicated effectively. Most petrologists and geochemists have concentrated on the endogenic phases, and their interest in the origin and chemistry of the Moon and of its early crust is reflected in the most commonly used lunar petrologic nomenclature. For example, names derived from terrestrial igneous petrology have been applied, inappropriately, to rocks melted and emplaced by impacts (Smith, 1974, p. 233; Irving, 1975, p. 364; Prinz and Keil, 1977). Stratigraphers are more interested in the times and processes of assembly and deposition of the breccia beds. These events in the rocks' histories are emphasized here and in the breccia-classification scheme discussed above in chapter 3 (Stöffler and others, 1979, 1980). The early crust is not described comprehensively here (see Taylor, 1982) but is treated mainly from the standpoint of its role as raw material for later stratigraphic units.

Unfortunately for those interested in the early Moon, no rocks of the early crust are preserved in outcrop, and only small fragments believed to be relatively unaltered samples of that crust have been recovered from the breccia deposits formed and emplaced by later impacts. Still more seriously for attempts to decipher the early Moon, no deposits identifiable with a specific pre-Nectarian stratigraphic unit were sampled. All the terra landings took place on Nectarian and Imbrian deposits because operational factors prevented Apollo and Luna from landing on the farside and southern nearside tracts where pre-Nectarian materials are exposed (pl. 6). Therefore, the photogeologically decipherable record and the sample record for the pre-Nectarian are connected much more tenuously than for later time-stratigraphic systems. Correlation of pre-Nectarian absolute and relative time scales and determination of the rates of impact and volcanic activity are difficult problems confronting stratigraphic and laboratory analysis.

CRUSTAL PETROLOGY AND GEOCHEMISTRY

Composition

The lunar terrae are composed of a crust of material that differentiated from the bulk Moon early in lunar history. The crustal composition was determined during early pre-Nectarian time by processes that are basically igneous, and was later mixed and otherwise modified by impacts. This mixing aids attempts to determine the average crustal composition, although it obscures whatever geochemical provinces may once have existed. Data from unmanned Surveyor analyses (Gault and others, 1968a; Turkevich and others, 1969; Phinney and others, 1970; Turkevich, 1971), returned-sample analyses, and orbital geochemical sensing (see chap. 5) currently combine to indicate an average terra composition rich in Al (25–29 weight percent Al_2O_3) and Ca (approx 14 weight percent CaO) (Taylor, 1975, 1982; Basaltic Volcanism Study Project, 1981, p. 666–678).

[8.1] To indicate that the pre-Nectarian system is not a formal stratigraphic name, the term is not capitalized (see introduction to the section in this chapter entitled "Basin and Crater Materials").

This chemistry is reflected in the low density of the crust (2.90–3.05 g/cm^3; Haines and Metzger, 1980; Basaltic Volcanism Study Project, 1981, p. 671) and in the fact that highly calcic plagioclase (mostly greater than 90 percent anorthite; Smith and Steele, 1975) is the most abundant sampled mineral. The next most abundant minerals in terra samples are low-Ca pyroxenes (mostly orthopyroxene, with subordinate pigeonite), olivine, and augite (high-Ca clinopyroxene). Aluminous or chrome spinel, ilmenite, silica minerals, troilite, and Fe metal are common accessories, and many other trace minerals are present (Smith, 1974; Frondel, 1975; Smith and Steele, 1975; Taylor, 1975, table 4.2; Cadogan, 1981, chap. 3). Lunar rocks vary far less in mode (optically visible minerals) and in mineral chemistry than do terrestrial rocks.

A series of rocks commonly called the ANT suite composes most of the returned terra material, where "ANT" refers to the plutonic-rock types *a*northosite (min 90 percent plagioclase), *n*orite (plagioclase and orthopyroxene), and *t*roctolite (plagioclase and olivine; table 8.1; Prinz and Keil, 1977; Stöffler and others, 1980). The plagioclase-rich composition of the terrae was first recognized in studies of small fragments in the Apollo 11 mare regolith (Wood, 1970; Wood and others, 1970), and the ANT suite was defined on the basis of small fragments in the Luna 16 and 20 regolith samples (Keil and others, 1972; Prinz and others, 1973; Taylor, G.J., and others, 1973; Prinz and Keil, 1977). Because the importance of impact mixing and melting was not fully appreciated during these early analyses, compositional types were commonly delineated incorrectly on the basis of mixed, brecciated, fine-grained, or even glassy rocks as if they were plutonic igneous rocks containing large optically identifiable crystals. The name "anorthosite" has been especially misused for materials that are not anorthosites in either the compositional or textural sense.

In ANT terminology, the "average" terra rock is an anorthositic norite or a noritic anorthosite (approx 70 percent normative plagioclase; Taylor, 1975, 1982). Unfortunately for the nonspecialist, this composition is also referred to as "highland basalt." This term was coined during study of regolith glasses (Reid and others, 1972a) and is one of several terms containing the word "basalt" that, especially in literature of the early 1970's, refer not to crystalline extrusive rocks but to magmas whose existence was predicted on the basis of glassy fragments (Apollo Soil Survey, 1971, 1974; Reid and others, 1972a, b; Prinz and others, 1973). Early workers commonly stated that "highland basalt" represents the most important primary magma of the terrae.

ANT rocks occur at all terra-sampling sites, though greatly varying in amount from the small fragments returned by Apollos 11, 12, and 14 and Lunas 16 and 20 to many kilograms from the Apollo 15, 16, and 17 landing sites. Earthlike granite and granodiorite are absent, but rare fragments of "granite" and "quartz monzodiorite" have been found (Ryder and others, 1975a; Ryder, 1976); these materials consist dominantly of quartz and potassium feldspar and contain varying amounts of relatively Fe-rich pyroxene and olivine and of relatively sodic plagioclase.

The most abundant type of highly differentiated lunar terra material is known, confusingly, by many partial synonyms, of which KREEP and KREEP-rich rock are the most nearly appropriate (table 8.1). The major-element composition of this material is not well defined, and the term refers primarily to an assemblage of minor and trace elements present in characteristic proportions (Meyer, 1977; Warren and Wasson, 1979c). The catchy acronym "KREEP" (coined by Hubbard and others, 1971, p. 343) refers to potassium (K), rare-earth elements (REE), and phosphorus (P); other diagnostic trace elements are Ba, Rb, Th, U, and Zr. These distinctive elements share the properties of large ionic radius (they are large-ion lithophiles [LIL]) and exclusion from the major mineral phases ("incompatible"). Although the name "KREEP basalt" commonly appears (Hubbard and Gast, 1971; Hubbard and others, 1971; Meyer and others, 1971), very few KREEP-rich samples have igneous textures. The term "KREEP" is properly used in a chemical, not a lithologic, sense for these diversely textured rocks. Major normative minerals of KREEP-rich materials are similar to those of the ANT rocks, except that plagioclase is more sodic (mostly less than An_{88}) and orthopyroxene and pigeonite are richer in Fe. Thus, both the minor- and major-mineral phases indicate advanced differentiation according to the Bowen (1928) reaction series. The incompatible elements are the longest to survive in residual liquids of magmas from which crystals have separated, and are the first to appear in new partial melts.

TABLE 8.1.—*Major-oxide compositions of major types of lunar terra material*

[All values in weight percent. Others, mostly TiO_2, Na_2O, K_2O, and Cr_2O_3 (Taylor, 1982, table 5.5); still other trace elements characterize KREEP (Warren and Wasson, 1979c). After Taylor (1975, p. 233-253; 1982, p. 201-233, tables 5.5, 8.2; S.R. Taylor, oral commun., 1982); data on high-K KREEP from Reid and others (1972b).
ANT: Compositions generally range from anorthosite (A, left) to norite (N, right) or, for MgO, to troctolite. Gabbro is synonymous with norite, except that high-Ca pyroxene characterizes gabbro and low-Ca pyroxene characterizes norite (Taylor, G.J., and others, 1973). In the terrae, low-Ca pyroxene is more abundant than high-Ca pyroxene.
KREEP: Compositions range from low-K (left) to high-K (right). KREEP-rich materials are also called KREEP basalt, Fra Mauro basalt (Reid and others, 1972b), nonmare basalt (Hubbard and Gast, 1971), high-Al basalt, alkali high-Al basalt (Prinz and others, 1973), norite (Wood, 1972a), KREEP norite, and many other names and acronyms (Taylor, 1975, p. 215, 272, table 5.8). Low-, medium-, and high-K KREEP-rich materials are commonly referred to as low-, medium-, and high-K Fra Mauro basalt (LKFM, MKFM, and HKFM, respectively).

Material----	ANT (A-N)	KREEP (low-high K)	Average terra
SiO_2--------	44-50	47-53	45.0
Al_2O_3-------	36-15	23-16	24.6
CaO---------	19-10	12-10	15.8
FeO---------	1-11	10	6.6
MgO---------	1-15	11-6	6.8
Others------	≤.7	≤3.5	≤1.2

A common classification recognizes three categories of KREEP-rich materials that are similar in major-element bulk composition but differ in the proportions of the distinctive minor elements, exemplified by potassium: high K (more than 1 weight percent K_2O), medium K (approx 0.5 weight percent K_2O), and low K (approx 0.1 weight percent K_2O)(Taylor, 1975, p. 234–237). Also, the Fe/Mg ratio and SiO_2 content increase as the K content increases. Low-K KREEP is the most abundant category and, in fact, may be the second most abundant component of the terra crust after the ANT suite (approx 20 percent; Taylor, 1975, p. 234, 252). Low-K KREEP occurs in glasses or fragment-laden impact melts in some abundance at all landing sites except the mare-dominated Apollo 11 site (James, 1980). It was first suggested as a magma type on the basis of glassy fragments (Reid and others, 1972b). As a legacy of the large Apollo 14 collection, these three categories of material are commonly called high-K, medium-K, or low-K Fra Mauro basalt (HKFM, MKFM, LKFM) (Apollo Soil Survey, 1971; Reid and others, 1972b). However, this volume avoids the term "basalt" for nonvolcanic rocks and restricts the name "Fra Mauro" to the rock-stratigraphic unit the Fra Mauro Formation.

Igneous or impact origin?

A petrologically and stratigraphically important question is how many terra rocks have compositions that result from igneous processes and how many have compositions that were assembled by impacts. Until about the time of the Third Lunar Science Conference in 1972, most investigators seemed to favor an origin of certain Apollo 14 samples with KREEP-rich compositions and textures indicating crystallization from melts as endogenic volcanic basalt ("Fra Mauro basalt"; fig. 2.8). The current consensus, however, is that almost all terra melt rocks with basaltlike textures originated as impact melts (Dence and Plant, 1972; Green and others, 1972; Taylor and others, 1972; James, 1973; Irving, 1975, 1977; McKay and others, 1978, 1979). The main clues are (1) trace elements indicating contamination by meteorites and (2) small-scale textural and compositional heterogeneity, especially among clasts.

Although impact-created rocks dominate the terrae, some igneous rocks from the early pre-Nectarian crust were recovered (fig. 8.2; Warren and Wasson, 1977, 1979b, 1980a, b; Norman and Ryder, 1979). A diligent search has been conducted for samples of these "pristine" rocks, which have also been referred to as meteorite-free, endogenic,

endogenous, indigenous, primitive, and plutonic (see references in Warren and Wasson, 1980a, p. 81–82). The following are the main criteria for pristinity that currently are most widely accepted.

1. A low content of *siderophile elements*, many of which are characteristic of iron meteorites and chondrites (for example, Hertogen and others, 1977; Morgan and others, 1977). The highly siderophilic elements Au, Ir, Os, Pd, and Re probably accompanied metallic Fe during early differentiation of Solar-System material and thus were concentrated in planetary cores and small Fe-rich bodies. A few investigators believe that the silicates of the Moon are intrinsically richer in these elements than is generally believed and that pristine rocks low in siderophiles are impact-melt rocks from which siderophiles have been removed by extraction of metal (Delano and Ringwood, 1978; Wänke and others, 1978). Most investigators, however, believe that high concentrations of these elements indicate meteoritic contamination, although their absence does not necessarily prove pristinity (Irving, 1975, 1977; Warren and Wasson, 1977; Anders, 1978; Norman and Ryder, 1979, p. 533–536; Taylor, 1982, p. 222).
2. Igneous, especially *cumulus*, textures. Impact melts rarely cool slowly enough to develop cumulus textures, which are conspicuous in layered intrusions on the Earth, where such factors as gravity, liquid density, and fluid currents have produced quasi-sedimentary features (Jackson, 1971; Jackson and others, 1975; Raedeke and McCallum, 1980). Thus, lunar cumulus textures indicate pristinity (fig. 8.2*D*). Such textures furthermore suggest that the rock's composition arose by igneous processes. In contrast, metamorphic textures commonly form in deposits of impact melt and breccia whose compositions arose by mechanical mixing of preexisting rocks. Volcanic textures may form either in true volcanic rocks or in impact melts, and thus are ambiguous when not supplemented by other clues, such as siderophile content.
3. Grain size larger than 3 mm, indicative of slow cooling in a plutonic environment. In many pristine samples, however, the original igneous textures and the coarse grain size have been obscured by subsequent shock-induced cataclasis.

It seems clear today that the bulk compositions of most terra rocks are determined by impact-induced mixing. Plots of bulk major-element compositions of lunar terra rocks reveal that individual endogenic cumulates and other pristine samples vary much more in composition than do obviously impact-generated polymict breccias and regoliths containing siderophiles (Warren and Wasson, 1977; 1979b, p. 601; 1980b; Norman and Ryder, 1979, p. 554; Taylor, 1982, p. 202). The "anorthositic norite" or "highland basalt" average terra composition, granulitic impactite (Warner and others, 1977; Bickel and Warner, 1978), very high alumina "basalt" (Dowty and others, 1973, 1974b; Hubbard and others, 1974), and low-K KREEP are among the compositional types that fall in the middle of such plots away from known pristine rocks. Low-K KREEP is found mostly (Ryder and others, 1977) or entirely in siderophile-bearing fragment-laden melts

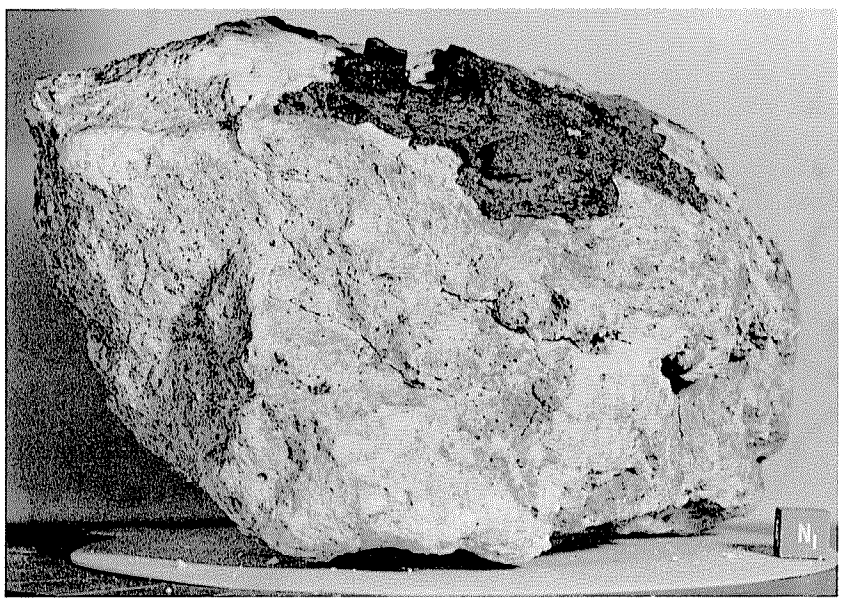

A

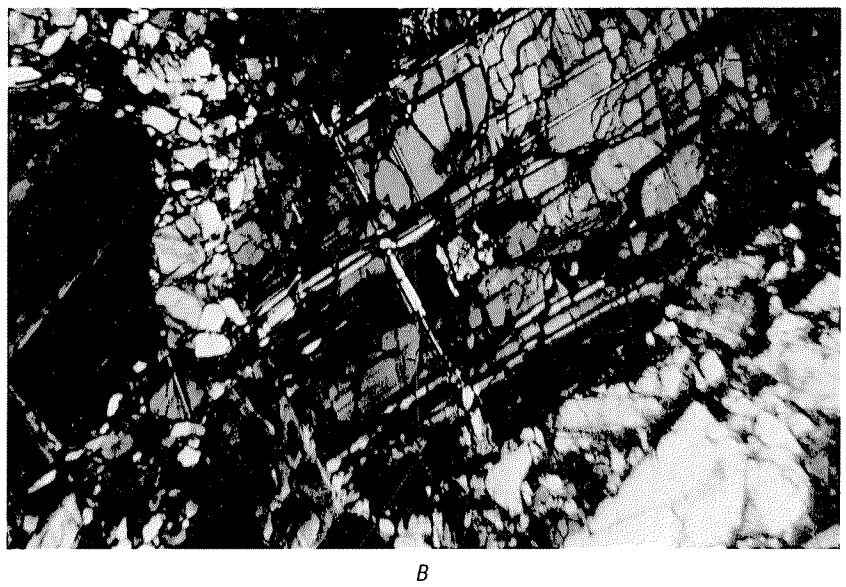

B

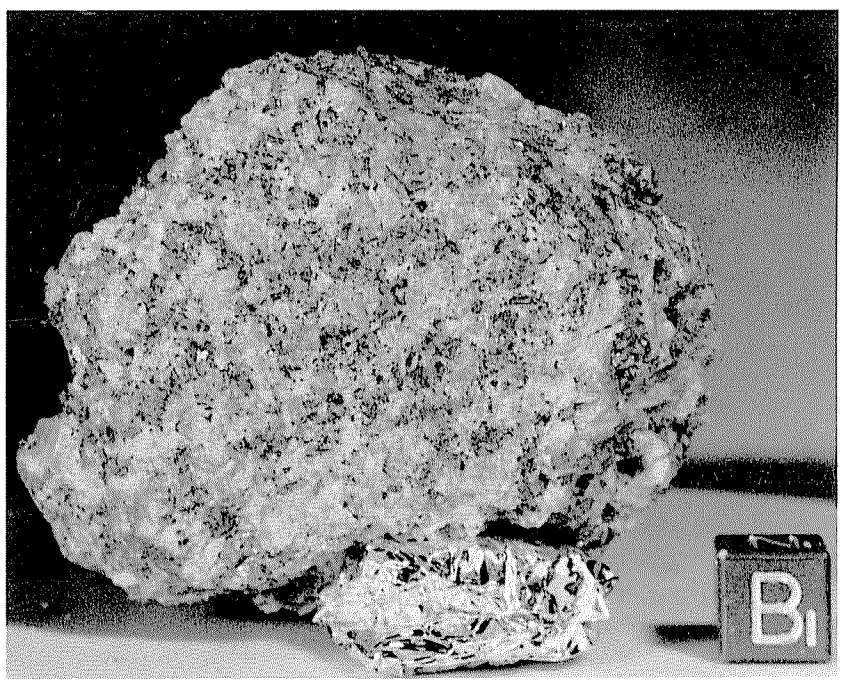

C

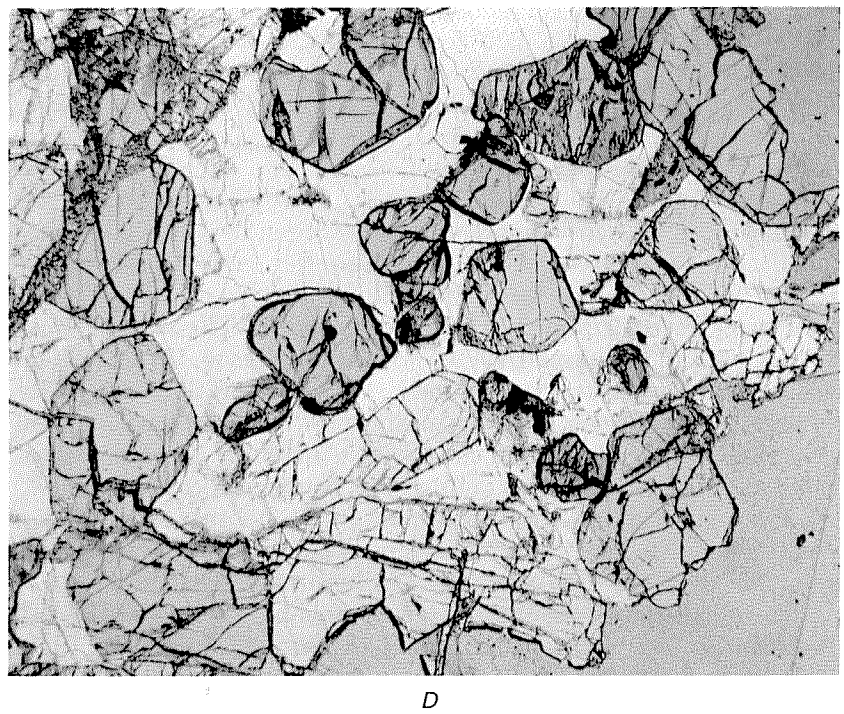

D

FIGURE 8.2.—"Pristine" terra samples.

A. Cataclastic anorthosite (sample 60025), as photographed in Lunar Receiving Laboratory after arrival from Apollo 16 landing site. Little texture is evident. Scale cube is 1 cm on a side in this and all other "mug shots."

B. Thin section of sample 60025. Most optically observable crystals (modes) are of plagioclase. Texture is seriate. Crossed polarizers; field of view, about 2 mm.

C. Coarse-grained granulitic troctolite (sample 76535) from North Massif, Apollo 17 landing site. Major modes are plagioclase (58 percent) and olivine (37 percent), with accessory orthopyroxene (4 percent) (Dymek and others, 1975).

D. Thin section of pristine pink spinel troctolite clast (sample 67435,14). Original igneous cumulate texture is largely preserved (Prinz and others, 1973). Euhedral to subhedral olivine (gray) is enclosed poikilitically by plagioclase (white). Plane-polarized light; field of view, about 2 mm.

(Meyer, 1977; Hess and others, 1977; McKay and Weill, 1977; Reid and others, 1977; Shih, 1977; Warren and Wasson, 1979b). This extensive impact mixing is to be expected from the geologic style of the Moon because each new impact mixes and melts rocks, most of which already are complex breccia deposits with compositions far removed from those of their endogenic origins. New hybrid compositions are formed by each event, and continued impacting creates a hybrid average of the original pristine compositions. Mixing models attempt to reconstruct the observed compositions of regoliths and bedrock-breccia deposits from a set of end members believed to represent original magma types (for example, Hubbard and Gast, 1971; Schonfeld and Meyer, 1972; see recent critiques by Ryder, 1979, and Taylor, 1982, p. 201–205).

In summary, the composition of the lunar terra crust was derived by mixing pristine ANT compositions with smaller amounts of highly differentiated KREEP-rich material. Although a few intact fragments of the early crustal rocks were recovered, the textures and structures of almost all returned terra samples were created by impacts. Many of the samples assembled by impacts retain the early endogenic compositions, whereas others have been compositionally as well as texturally altered during the impact reworking. Problems still persist in identifying the sources of specific samples and determining the relative amounts of pristine and impact-mixed materials. However, enough clues about the early crust have been assembled from this obscure record to reconstruct the following partial plutonic history of the early crust.

EARLY CRUSTAL PETROGENESIS

Magma ocean

Analysis of the small fragments from the Apollo 11 regolith led to what is still the leading model for the origin of the early crust (Smith and others, 1970; Wood and others, 1970). The terra crust and the mantle source of mare-basalt magmas are widely thought to have separated from a very large volume of magma popularly called a *magma ocean* (Walker and others, 1975; Wood, 1975b). The first hint of an early widespread differentiation of primitive materials came from REE abundances. Europium is overabundant in "average" terra rocks and underabundant in mare basalt relative to chondritic REE abundances (for example, Taylor, G.J., and others, 1973; Smith, 1974; Taylor, 1975, p. 154–159). This relation is consistent with an efficient mechanical separation of the ultramafic mare-source material, as cumulates, from a magma from which large amounts of plagioclase had already crystallized and extracted Eu relative to the other REE's. Plagioclase has large lattice sites that accept the large divalent (reduced) ion that only Eu among the REE's possesses.

"Oceanic" depths of 200 to 400 km are commonly favored, although lesser or greater depths are not excluded (half the lunar volume lies above, and half below, 360-km depth) (Walker and others, 1975; Hubbard and Minear, 1975; Herbert and others, 1977; Taylor, 1978; Longhi, 1980; Binder, 1982). Because of its lesser density, the plagioclase-rich terra-crustal material presumably floated in the magma ocean, whereas ultramafic cumulus crystals sank to form the upper mantle that became the mare source (for example, Smith and others, 1970; Wood and others, 1970; Taylor and Jakeš, 1974; Taylor, 1975, 1978; Wood, 1975b, c; Herbert and others, 1977; Ryder and Wood, 1977; Longhi and Boudreau, 1979; Warren and Wasson, 1979a, 1980a). The divide between the sunken and floated materials is generally assumed to be the seismic discontinuity at the base of the crust. If the ocean was 360 km deep and the crust is 75 km thick, the crustal material constituted about a quarter of the original oceanic volume.

The origin of KREEP in general and its role in "magma oceanography" in particular have generated a very large literature because of its persistent appearance in lunar samples and its exotic highly differentiated chemistry (see reviews by Taylor, 1975, 1982; Irving, 1977; Meyer, 1977; Warren and Wasson, 1979c; James, 1980; Vaniman and Papike, 1980). Its origin has been ascribed to partial melting of ANT material or, as commonly in more recent literature, to a late stage in fractionation of the magma ocean. KREEP has been considered to be derived from a minor liquid accumulated in dispersed niches throughout the magma ocean or the crust, or, alternatively, concentrated in certain regions. The question of its origin is difficult to resolve because because most or all analyzed KREEP is a chemical constituent incorporated into other rocks, rather than a distinct rock type itself.

Multiple plutons

Study of pristine rocks, many of which are thought to be relics of the primordial crustal differentiation, has shown that the magma-ocean model outlined above is too simple. Many of the pristine crustal rocks, especially those from the Apollo 17 landing site, are cumulate norite and troctolite that apparently formed by settling in their parent magmas (Norman and Ryder, 1979, p. 538). Data from the orbital geochemical instruments, as interpreted by mixing models, indicate that the topmost part of the "average" crust can contain no more than about 60 percent anorthosite (Haskin and Korotev, 1981) and that compositions range laterally from highly feldspathic to highly mafic (Spudis and Hawke, 1981). Moreover, the orbital instruments covered only a small percentage of the Moon and are subject to calibration problems (see chap. 5). Therefore, mafic materials may be more abundant than once thought.

Compositional subtleties of the mafic and anorthositic ANT rocks suggest that more than one magma system may have built the terra crust. For example, if the Mg/(Mg + Fe) ratios in mafic minerals (olivine, pyroxene) in the pristine rocks are plotted against the Ca/(Ca + Na + K) ratios in plagioclase, two distinct trends are definable (fig. 8.3; Steele and Smith, 1973; Taylor, G.J., and others, 1973; Warner and others, 1976; Warren and Wasson, 1977, 1979a, b, 1980a; Wood, 1977; Binder, 1980; James, 1980; Longhi, 1980; Raedeke and McCallum, 1980; Taylor, 1982, p. 248–251). One trend consists of highly feldspathic rocks (anorthosite and troctolitic anorthosite) that contain relatively calcic, uniform plagioclase and relatively Fe-rich, compositionally varying mafic minerals; these rocks are termed *ferroan anorthosite* because of the Fe-rich mafic minerals (Dowty and others, 1974a). The other trend consists of more mafic rocks (troctolite, spinel-bearing troctolite, norite, gabbronorite, and a few ultramafic rocks) that have highly varying plagioclase and relatively magnesian, compositionally varying mafic minerals; these rocks are referred to as Mg-rich plutonic rocks or the *Mg suite*. In an individual rock of the Mg suite, Mg-rich mafic minerals are associated with Ca-rich plagioclase, and Fe-rich mafic minerals with more sodic plagioclase. These associations are what is to be expected in typical cotectic igneous differentiation (Bowen, 1928). The anorthosite was at first thought to be more anomalous (McCallum and others, 1975)

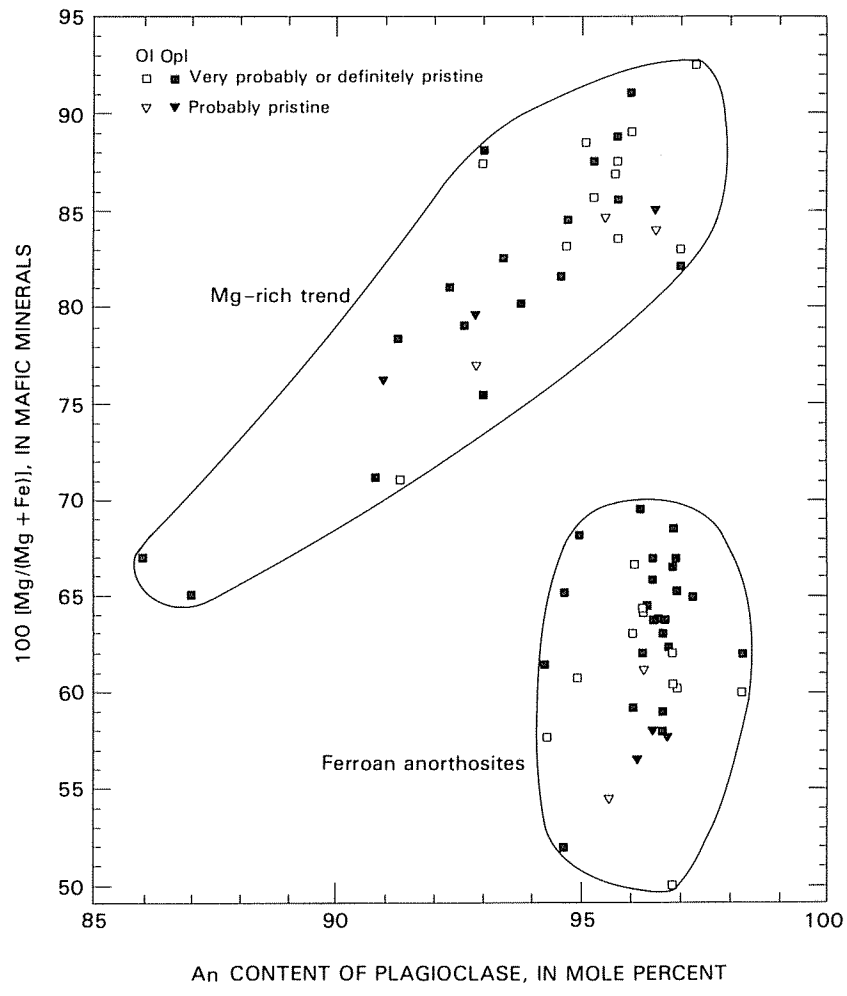

FIGURE 8.3.—Ferroan-anorthosite and Mg-rich trends in ANT rocks, separated by a distinct hiatus. Examples shown are for olivine (ol) and orthopyroxene (opx) in pristine rocks (Warren and Wasson, 1980a).

because Fe-rich mafic minerals are associated with Ca-rich plagioclase (Wood, 1975b; 1977, p. 48). However, the same type of mineralogic variation has been discovered in anorthosite of the Stillwater layered igneous complex (Raedeke and McCallum, 1980). No simple magma system is likely to have generated both trends simultaneously (Wood, 1975b; Longhi and Boudreau, 1979; Warren and Wasson, 1979a, b, 1980a, b; Raedeke and McCallum, 1980).

To accommodate the intricacies and the global scale that both seem required, several authors have proposed "separate pluton" models, in which layered Mg-suite plutons (Jackson and others, 1975; Raedeke and McCallum, 1980) intruded from below into an already-floated crust of ferroan anorthosite (Binder, 1980; James, 1980; Warren and Wasson, 1980a). Alternatively, the early pre-Nectarian crust may never have been an "ocean" but only a system of magma "pods" or "ponds" (Wetherill, 1975b, 1976; Simonds, 1979). Complex petrologic schemes dating from the accretionary period (Simonds, 1979; Smith, 1982) or operating in an early convecting magma ocean (Longhi, 1980) have also been proposed. Impacts must have bombarded the primitive Moon catastrophically; they would have pierced any solid crust that formed on an "ocean" and have stirred and mixed the liquid, influencing the early geochemistry and petrogenesis (Wetherill, 1975b; Wood, 1975b; Hartmann, 1980; Minear, 1980; Simonds, 1979; Warren and Wasson, 1980a; Taylor, 1982, p. 248–251). Although the magma-ocean concept is still favored by most petrologists and geochemists, it is becoming increasingly modified and complex.

Crustal zonation

Possible layering or, more likely, crude vertical zonation of the crustal material has been studied by a combination of seismic, petrologic, and impact investigations. Seismic data indicate a discontinuity in the crust at about 20- or 25-km depth (Toksöz, 1974; Toksöz and others, 1974; Goins and others, 1979) that is commonly ascribed to an interface between low-density, relatively porous crustal rock and denser sealed material of the same composition (Todd and others, 1973; Bills and Ferrari, 1977; Haines and Metzger, 1980). Alternatively, or additionally, this seismic feature could represent a compositional discontinuity between more feldspathic material above and more mafic material below (Herzberg and Baker, 1980; Warren and Wasson, 1980a). A distinct KREEP-rich layer has also been suggested, either between layers of anorthosite and more mafic material (Ryder and Wood, 1977) or at the base of the crust (Warren and Wasson, 1979c).

Because basins probe the subsurface, the surface distribution of ejecta compositions should help in reconstructing any layering or zonation that exists. The large size of basins might suggest excavation as deep as the mantle. Mineral assemblages in some spinel-bearing Mg-suite rocks have been cited as requiring pressures available only in the deep crust or mantle of the Moon (Herzberg, 1978; Herzberg and Baker, 1980). However, alternative phase-equilibria schemes allow an origin as shallow as 25 km, well within the crust (Warren and Wasson, 1979a; Herzberg and Baker, 1980). Although most terrestrial dunite is probably of mantle origin, at least one Mg-suite lunar dunite probably originated in the crust, judging from its association with, and mineralogic similarity to, troctolite sample 76535, whose cooling and reequilibration depths were probably in the range 10–30 km (Gooley and others, 1974; Dymek and others, 1975). Orbital geochemistry suggests crustal composition even for Imbrium-basin ejecta, which I believe was derived from the cavity of the Moon's largest known basin, Procellarum (fig. 8.4). Therefore, little, if any, mantle material was brought to the surface in impact ejecta, and shallow basin excavations restricted to the crust are implied.

Crustal thickness and surface composition seem to be related; the more aluminous the material, the thicker the crust (Schonfeld, 1977; Haines and Metzger, 1980). That is, the Pratt (unequal density) model of isostasy seems to be more nearly applicable to the terrae than is the Airy model (Solomon, 1978). The Airy (equal density) model was assumed in arriving at the commonly stated conclusion that the farside crust is thicker than the nearside crust (Kaula and others, 1974). Most investigators have nevertheless concluded that the farside crust is thicker (see chap. 1), even under Pratt or mixed isostatic models (Haines and Metzger, 1980).

This difference in crustal composition and thickness, however, may not be hemispheric in extent. The orbital geochemistry (Haines and Metzger, 1980) suggests that the crust is both thinner and more magnesian beneath the two largest lunar basins, Procellarum and South Pole-Aitken, than in other regions where data are available. Seismic data (see chap. 1) suggest that the crust is 50 or 60 km thick under southern Oceanus Procellarum and about 75 km thick under the highly feldspathic Apollo 16 landing site, which is near the Procellarum rim (pl. 3). Crustal thicknesses are similar on the southern nearside and western (long 90°–180° E.) farside (fig. 1.12; Bills and Ferrari, 1977). The X-ray spectrometer detected higher Al/Mg ratios on the farside and on parts of the eastern and southeastern nearside than in the Imbrium-Procellarum region (Adler and others, 1972, 1973; Hubbard and others, 1978). No data known to me contradict the conclusions that the thick aluminous crust is restricted to the rims and exteriors of the two giant basins and that the thinner, more magnesian crust is concentrated in basin interiors. Additionally, the gamma-ray spectrometer detected the high radioactivity characteristic of KREEP in the Imbrium-central Procellarum region (Metzger and others, 1973, 1977), where I would expect the thinnest part of the lunar crust.

The sample data support the conclusion that the giant basins control the crustal thickness and, thus, the compositional zone that was accessible to later impacts (fig. 8.4). The greatest depths were reached by the Imbrium basin, whose ejecta (Fra Mauro Formation) is correspondingly the lunar deposit richest in KREEP (see chap. 10). Mg-suite rocks and low-K KREEP, probably derived from the same or shallower depths, apparently compose most of the Imbrium (Apollo 15; chap. 10) and Serenitatis (Apollo 17; chap. 9) rims. The Apollo 16 and Luna 20 landing sites are the richest in feldspathic ANT materials (chap. 9), as befits their derivation from the thick crust of the outer Procellarum shelf or exterior terrain.

This picture, though internally consistent, is subject to revision or rejection on the basis of better data. Lateral zonation of primordial origin also is possible. Only four major sample suites from four landing sites have been collected from the terrae, and each suite added complicating detail to the lunar petrogenetic picture. On the basis of the complexities generally uncovered when geologic systems are examined closely, fine-scale local intrusions only crudely organized into petrologic provinces might be expected. The pattern that seems to reflect global layers exposed by large basins might be fortuitous.

BASIN AND CRATER MATERIALS

Introduction

The severely deformed, chemically and texturally mixed, siderophile-rich materials found in the Nectarian and Imbrian deposits attest to a high rate of impacts during pre-Nectarian time as well. More specific information on the characteristics of individual pre-Nectarian units is sparse because none were sampled directly and because the chemical and petrologic criteria for recognizing such units are ambiguous. Attempts have been made to identify individual impacting projectiles with specific basins by means of distinctive siderophile signatures (Hertogen and others, 1977; Morgan and others, 1977), but the success of these attempts is limited by knowledge of the prebasin stratigraphy. The study of pre-Nectarian impact deposits thus requires stratigraphic analysis.

Originally, pre-Nectarian and Nectarian were combined as pre-Imbrian (Shoemaker and Hackman, 1962). This designation sufficed for most old units mapped at 1:1,000,000 scale because the mapping was confined to the central nearside, which is dominated by the Imbrium basin (pl. 3). If they were subdivided at all, pre-Imbrian craters were numbered according to the morphologic criteria established by Pohn and Offield (1970).

The desirability of stratigraphically dividing the pre-Imbrian emerged during mapping of the nearside regions farthest from Imbrium. While mapping south of Mare Nectaris, Stuart-Alexander (1971) recognized a lineate surface as the expression of Nectaris-basin deposits and secondary-impact craters similar to those of the Orientale and Imbrium basins (fig. 8.5); she named the deposit the "Janssen Formation" (Stuart-Alexander, 1971). At first, the Janssen was used to subdivide pre-Imbrian crater materials into numbered pre- and post-Nectaris categories descendant from Pohn and Offield's

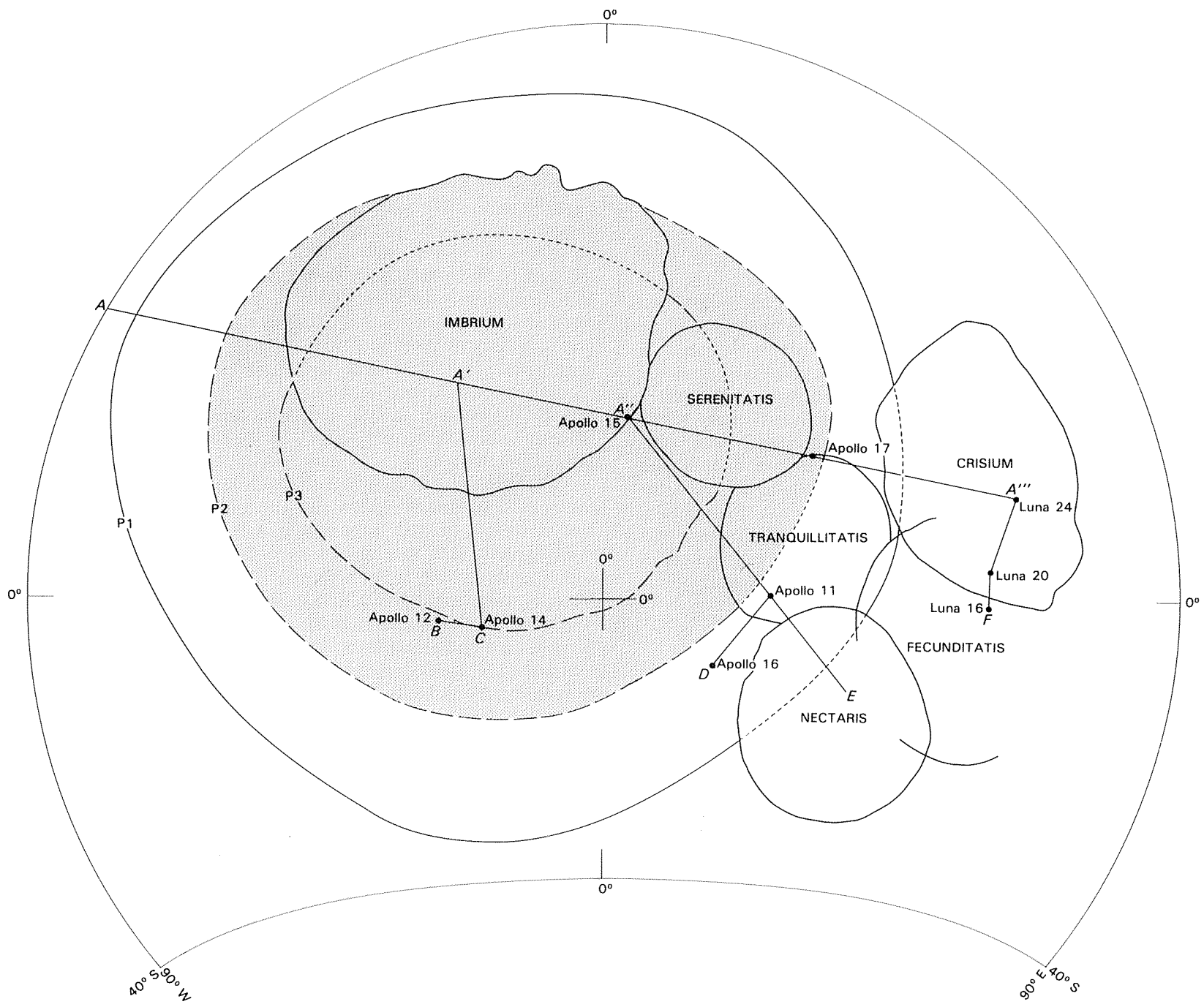

A

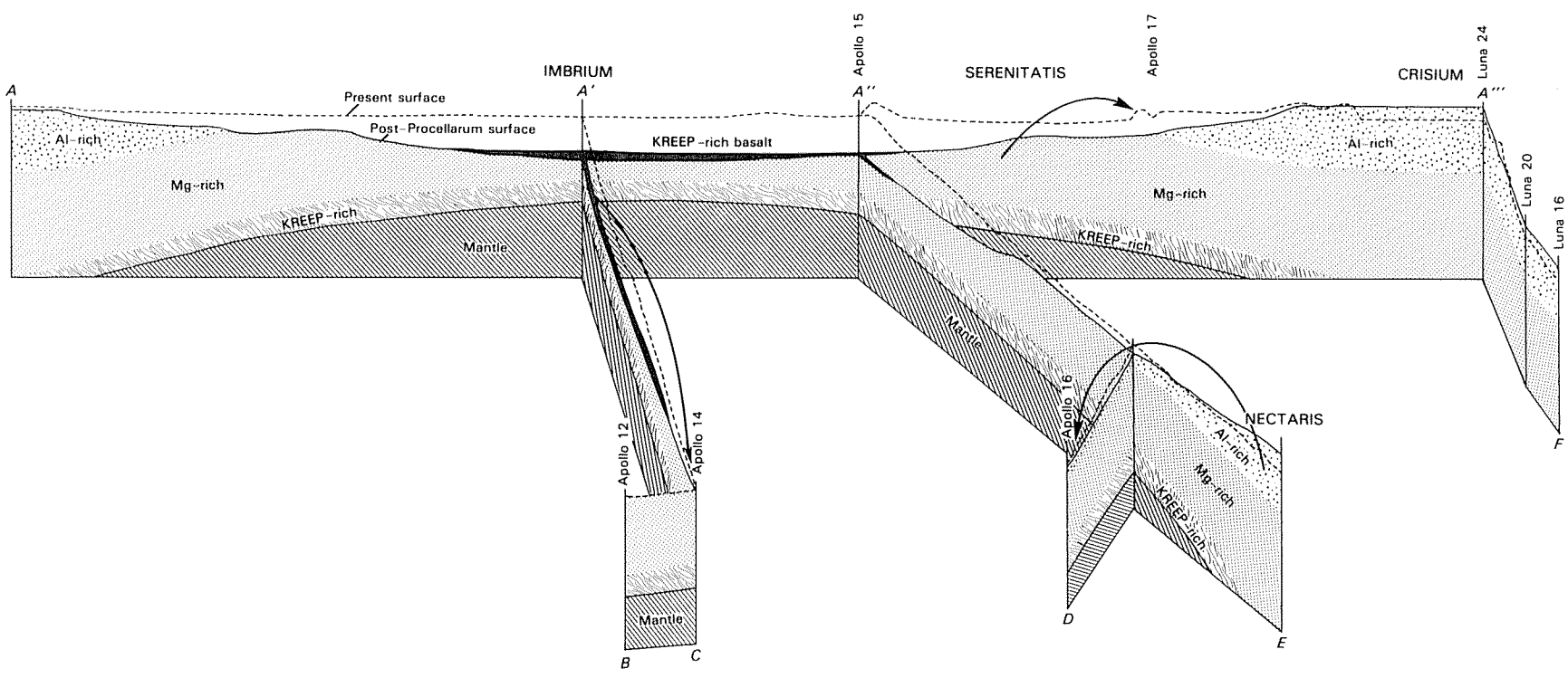

B

FIGURE 8.4.—Hypothetical crustal layers intersected by impact basins.

A. Index map based on plate 3, showing basins from which samples were obtained. P1, P2, P3, rings of Procellarum basin (dotted where inside younger basins; inner rings dashed). Shading, Mg-rich terrane after formation of Procellarum and before formation of other basins.

B. Diagrammatic geologic fence diagram, suggesting crustal and mantle configuration after Procellarum impact, subsequent uplift, and partial fill by hypothetical KREEP-rich volcanic basalt (black). Three gradational crustal layers are intersected by Procellarum-basin surface: upper Al-rich material is exposed outside basin and on outermost shelf (between P1 and P2); Mg-rich material is exposed on intermediate shelf (between P2 and P3) and in central basin; and lower-crustal KREEP-rich material is near surface (or may be exposed) near center of basin. Nectaris and Crisium basins were formed mostly in Al-rich terrane (Apollo 16 and Luna 20 samples, respectively); Serenitatis basin was formed in Mg-rich terrane (Apollo 17 samples); Imbrium basin was formed in Mg-rich terrane (Apollo 15 samples) and also ejected large amounts of KREEP-rich material and (or) KREEP-rich basalt (Apollo 14 samples). Arrows indicate paths of ejecta. Curvature of surface trace and of the Moon is ignored; vertical exaggeration is arbitrary.

numeric designations (Stuart-Alexander, 1971; Wilhelms and McCauley, 1971; Scott, 1972b). In 1975, the pre-Imbrian was formally divided into the pre-Nectarian and Nectarian (Stuart-Alexander and Wilhelms, 1975). This division is shown on all subsequently published geologic maps, where appropriate, and is used here. The utility of this subdivision was proved as the limb, farside, and polar regions were mapped further and large numbers of pre-Nectarian and Nectarian units were identified (Scott and others, 1977; Wilhelms and El-Baz, 1977; Lucchitta, 1978; Stuart-Alexander, 1978; Wilhelms and others, 1979). The term "pre-Imbrian," however, is still used where more convenient, as in places on the nearside where the finer distinction cannot easily be made. Because neither "pre-Nectarian" nor "pre-Imbrian" has a formally defined base, such terms as "system" and "period" used in conjunction with them are informal and not capitalized.

Recognition criteria

A start in establishing a pre-Nectarian age is to examine terrain covered by the deposits and secondary craters of the Nectaris basin (fig. 8.5). Deposits overlain by these materials are, by definition, pre-Nectarian. Pre-Nectarian basins in direct contact with Nectaris-basin materials include Australe, Fecunditatis, Mutus-Vlacq, Tranquillitatis, and Werner-Airy (pl. 6; table 8.2). Craters lightly nicked by Nectaris secondaries but not deeply buried by deposits are type examples of pre-Nectarian craters (figs. 8.5*C*, *D*).

Units not in contact with Nectaris-basin materials can potentially be dated by comparing the size-frequency distributions of superposed primary craters with those of craters superposed on Nectaris (fig. 8.6; table 8.2). Size-frequency curves lying entirely above that for Nectaris demonstrate a pre-Nectarian age. One curve for a basin here considered to be pre-Nectarian (Apollo) crosses below the Nectaris curve, but only at the statistically weak end representing the frequencies of large craters.

The differences among the many curves demonstrate the fact that the lunar terrae do not have some single characteristic size-frequency distribution but are composed of basin blankets, each of which has reset the visible crater population of the surfaces it covers. The slopes of the cumulative crater-frequency curves decrease and become more highly curved from the youngest to the oldest surfaces (fig. 8.6). Some of the crater-frequency curves approach a slope of -1 for craters as large as 60 or 70 km in diameter, a slope substantially lower than that of -2 or -1.8 which is commonly believed to represent the production frequency for younger craters (for example, Basaltic Volcanism Study Project, 1981, chap. 8). Although the -1 slope has not been modeled in studies of crater saturation (Woronow, 1977, 1978), it nevertheless probably results from mutual obliteration of pre-Nectarian and Nectarian craters.

Several factors in addition to this destruction of craters limit the counts to craters at least 20 km in diameter. Meaningful counts are restricted to (1) superposed craters and (2) primary craters. A superposed crater useful in dating the basin, and a subjacent crater whose inclusion in the counts would be erroneous, may differ only slightly in appearance. Numbers of secondary craters generally do not indicate time of exposure because such craters are generated in bursts when their parent primaries form. The superposed-buried and primary-secondary distinctions can be made only in well exposed, well photographed terrains. Some counts of pre-Imbrian craters are inevitably restricted to small areas because of burial by later deposits; the buried craters are visible but are useless for dating (fig. 8.7). Photographic quality on the farside is inadequate for interpreting craters smaller than 20 km in diameter on many basins, especially at latitudes poleward of about 40°.

The results of these natural and artificial shortcomings are indistinct separations of the curves for old basins and statistically poor curves for the smallest and the youngest (least cratered) units. No individual craters are dated here by crater densities except the 265-km-diameter crater-basin transitional feature Milne (figs. 4.2*J*, 8.11). For most pre-Nectarian craters, the small superposed craters that are required for statistically significant counts have been erased by mutual obliteration and degradation on slopes. Several counts of superposed craters are listed in table 8.2 as "poor," meaning that they contain few total craters or lack small craters because of burial. These counts are not plotted in figure 8.6 except for the marginally useful one for the Coulomb-Sarton basin.

Pre-Nectarian surfaces may be heavily or only moderately cratered, depending on age and happenstance position relative to younger secondary clusters. Although densities of superposed secondary craters are almost useless for dating, clustered secondaries are very useful for establishing relative age if they can be traced to their source basins (fig. 8.7*A*). Once a basin is established as pre-Nectarian, superposition of its secondary clusters on another basin or crater unit establishes the pre-Nectarian age of that unit as well. Where available, superpositions prevail over crater counts as age criteria. Secondary clusters can also be used to date small units, such as those of individual pre-Imbrian craters that are inaccessible to size-frequency studies. Numerous stratigraphic relations between pre-Nectarian and younger basins and between pre-Nectarian basins have been established by such superpositional relations (table 8.2).

Basins

This volume divides 30 pre-Nectarian basins into 9 age groups (table 8.2). Each group is headed by one basin whose relative age seems to be well established by crater densities or superpositional relations. Additional basins are tentatively placed in the groups on weaker grounds.

The first group consists of the giant South Pole-Aitken and Procellarum basins. South Pole-Aitken is characterized by saturation of superposed impact structures as large as basin size (fig. 8.8; table 8.2). The history of its discovery illustrates the need for mapping large areas. When Hartmann and Kuiper (1962) realized that basin rings are prevalent on the Moon, they predicted the presence of a large farside basin on the basis of telescopic photographs showing huge mountains near the Moon's south pole. This prediction went unnoticed when Soviet Zond photographic altimetry and Apollo laser altimetry revealed a large depression as much as 5 to 7 km below the average farside surface (see review by Stuart-Alexander, 1978). Some massifs had been photographed by Apollo 8, but their connection with a basin was not immediately perceived (fig. 8.9; Wilhelms and others, 1969). Wilhelms and El-Baz (1977) mapped other massifs without knowing of their connection with the basin. Several observers then independently discovered that mountains over a huge area of the southern farside and southernmost nearside form a giant ring (pls. 3, 6; fig. 8.8; Howard and others, 1974; Schultz, 1976b, p. 306; Stuart-Alexander, 1978; E.A. Whitaker, written commun., 1976). Now, there is little doubt about the existence of this "Big Backside Basin," although the number and exact diameters of the rings are uncertain (Wilhelms and others, 1979).

Regional studies also suggest the presence of the Procellarum (Whitaker, 1981) or "Gargantuan" (Cadogan, 1974, 1981) basin. Some of the profound effects of this 3,200-km-diameter basin (pl. 3; fig. 8.10; Whitaker, 1981) on the later geologic evolution of the Moon have already been described. (1) Its excavation thinned the crust considerably, possibly by 50 km, and the mantle rose in isostatic compensation (figs. 6.22, 8.4). (2) As a result, the terra surface was lower, and the elastic lithosphere thinner or weaker, during mare extrusion and structural deformation in the Procellarum region than elsewhere on the Moon. (3) Their relation to Procellarum accounts for numerous concentric ridges and troughs of the terrae, which, like the mountains now known to be parts of South Pole-Aitken, would be anomalous if not part of a basin (fig. 8.10). (4) Redistribution of crustal materials by the Procellarum impact may be an important factor in the distribution of anorthositic, Mg-suite, and KREEP-rich terra materials (fig. 8.4). (5) More speculatively, Procellarum ejecta and, possibly, ejecta of the South Pole-Aitken basin may account for the suggested thickening of the farside crust (Cadogan, 1974; proposed previously in somewhat different form by Wood, 1973). (6) The Procellarum basin is the reason for the existence and circular shape of Oceanus Procellarum (pl. 4; fig. 5.26), which otherwise would have had to form by a special "continental" type of mare-basalt volcanism otherwise unknown on the Moon. (7) Other maria, contained in basins superposed on Procellarum, are more numerous, larger, and deeper than maria in equally large or larger basins outside Procellarum (pl. 4). (8) Isostatic compensation has gone further inside Procellarum than on the thicker lithosphere outside. (9) More uplifted crater floors lie in and near Procellarum than elsewhere (pl. 5). (10) Arcuate rilles, opened by mare subsidence, are abundant inside but rare outside the basin (pl. 5); straight rilles may also be controlled by this largest lunar feature (see chap. 6). Additional effects of Procellarum on mare volcanism are described in chapters 11 through 13.

Age group 2 (table 8.2) rather arbitrarily consists of eight basins whose existence is uncertain; their collection into a single group is based on the assumption that if these basins were younger (and if they exist), they would be more obvious. The −1 slope of the cumulative size-frequency distribution of the numerous craters counted on Al-Khwarizmi/King (figs. 8.6, 8.11) characterizes that ancient basin. If this basin does not exist, the −1 slope characterizes other ancient lunar terrane, possibly South Pole-Aitken deposits, which probably extend into this region. Two of the age-group 2 basins, Flamsteed-Billy and Insularum, were identified on the basis of circular patterns of terra islands in the western maria (pl. 3; fig. 8.10; Wilhelms and McCauley, 1971). This criterion for basin identification arose from the discovery that seemingly isolated elevations generally are parts of basin rings.

The basins of age groups 3 and 4 are also so heavily degraded that they have lost most traces of ejecta, and superposed and prebasin craters are difficult to distinguish in their peripheries. Nevertheless, they are still likely to be true basins. Saturation by large craters appears to affect the size-frequency plots significantly; the slopes of some curves for craters believed to be superposed approach −1. Because of this saturation or deep burial by later basin or mare deposits, ranking of basins by age within one of these older groups is not considered feasible, even where crater frequencies appear to differ substantially (for example, Lomonosov-Fleming versus Mutus-Vlacq).

Identification of Mutus-Vlacq and Lomonosov-Fleming as basins is another result of mapping with the impact model in mind. Extensive tracts of "pitted plains" of pre-Imbrian age are concentrated southwest of the Nectaris basin (pl. 7; Wilhelms and McCauley, 1971; Scott, 1972b). These plains are centered within a partial circle of massifs and ridges (fig. 8.12; Wilhelms and others, 1979). This concentration of plains suggests the presence of a basin, Mutus-Vlacq, regardless of the plains' origin (see chap. 9). Some of the Mutus-Vlacq massifs had been identified in earlier mapping but were considered to be "volcanic domes" (Wilhelms and McCauley, 1971; Mutch and Saunders, 1972) before the Apollo 16 results downgraded the significance of terra volcanism. Similarly, Lomonosov-Fleming was identified by mapping mounds, ridges, and scarps that form a circle 620 km across and that encompass extensive light-colored plains (fig. 8.13; Wilhelms and El-Baz, 1977). Although no interior ring is observed in either of these basins, the term "ringed basin" is appropriate because the presence of another ring or rings beneath the plains fill is predictable by analogy with better exposed basins.

Although the indistinct Nubium, Fecunditatis, and Tranquillitatis basins cannot be accurately dated by superposed craters, they are subjectively ranked with the other age-group 3 basins on the supposition that they would be equally conspicuous if not flooded by mare materials. Fecunditatis probably has at least two exposed and one buried ring and thus has the most elaborate visible ring structure of the poorly observed basins listed in table 4.2. The 680-km-diameter ring, overlain by the young fractured-floor crater Taruntius (Wilhelms, 1972b), is the most conspicuous, but another ring, about 980 km in diameter, is probably the main topographic rim.

Age group 4 consists of three well-established basins. The diameters, numbers of rings, and age relations of Keeler-Heaviside and Ingenii, however, are somewhat uncertain because several nearby massifs may belong to the South Pole-Aitken basin (figs. 1.4, 8.7).

Although the two basins assigned to group 5 are poorly photographed or obscured by younger deposits, their deposits apparently have diminished the crater densities within a basin radius or diameter of the rim, as expected around basins. Smythii contains a distinct mare (fig. 8.11) and a mascon (table 6.1) but has only indistinct rings. Coulomb-Sarton (figs. 4.3*M*, 8.14) was discovered shortly after photography of the farside by the Lunar Orbiter spacecraft and was designated "unnamed basin B" (Hartmann and Wood, 1971). The rings are vague, and the identity of the topographic rim uncertain (table 4.1). Wood and Head (1976) withdrew the basin from the list of lunar basins. Massifs and abundant interior plains do exist, however, and the basin is here considered to be definitely established (Lucchitta, 1978).

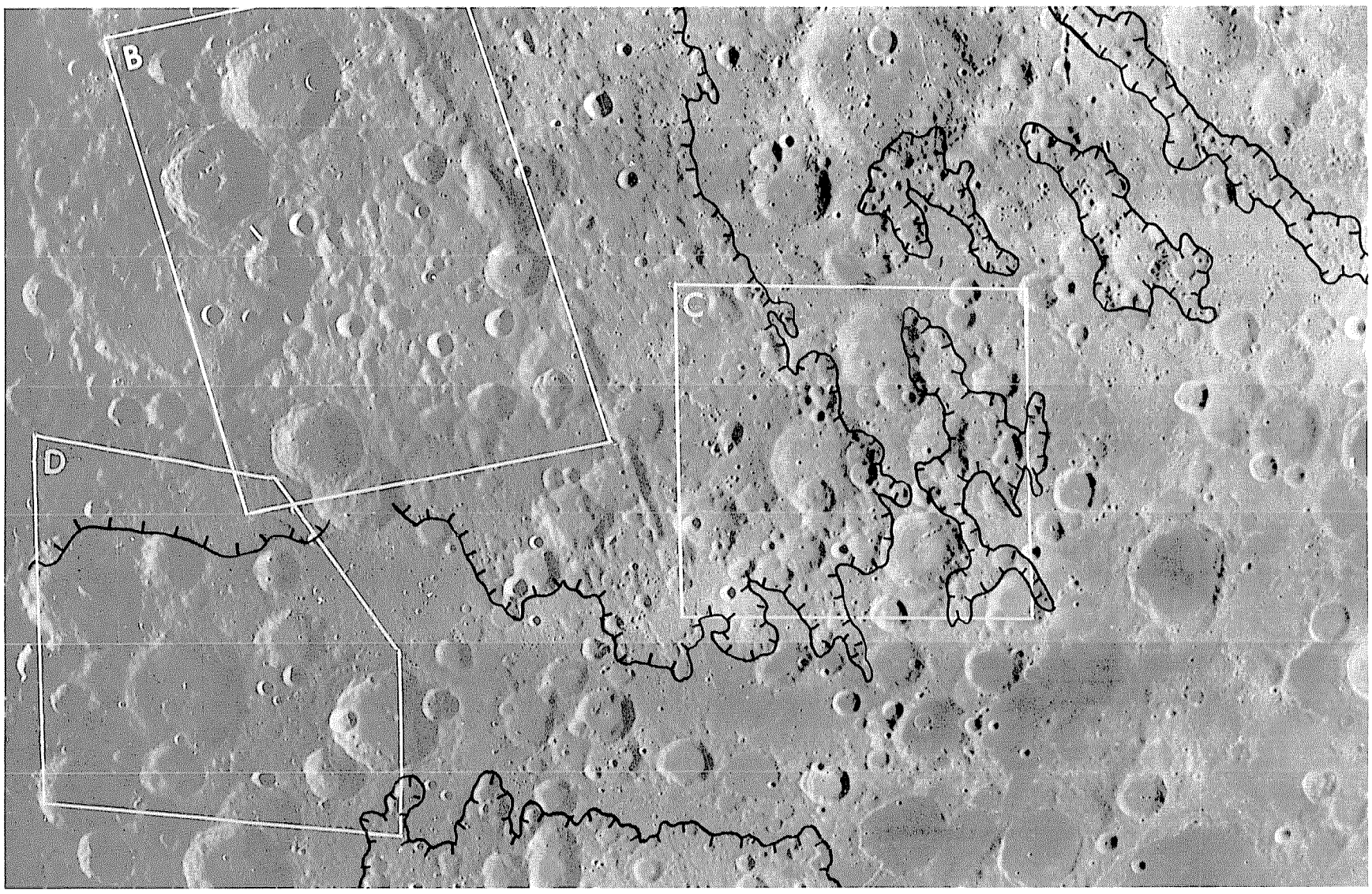

FIGURE 8.5.—Boundary between pre-Nectarian units and Nectarian System southeast of Nectaris basin (Stuart-Alexander, 1971; Stuart-Alexander and Wilhelms, 1975; Wilhelms and El-Baz, 1977; Wilhelms and others, 1979).

A. Regional view showing concentrations of textured deposits and secondary craters of Nectaris basin (hachured black outlines) and areas of *B* through *D* (white outlines). Orbiter 4 frame M–52.

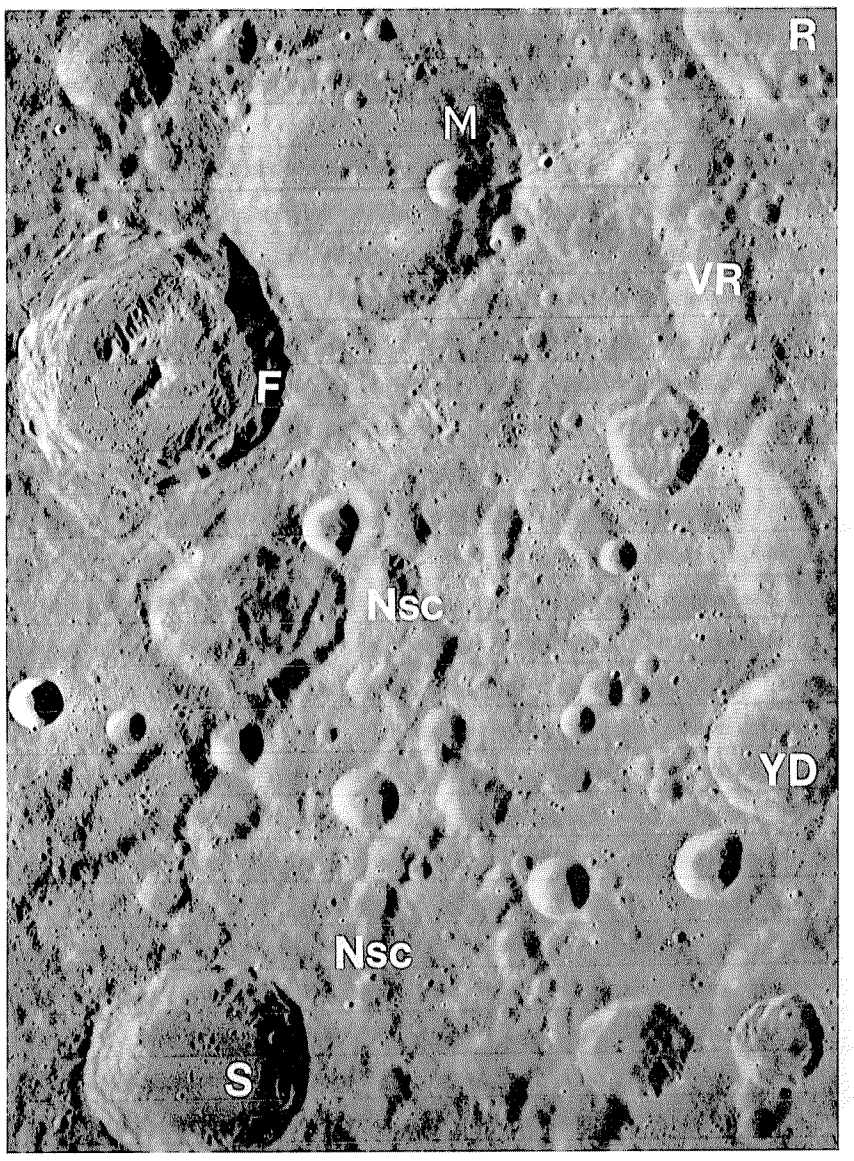

B

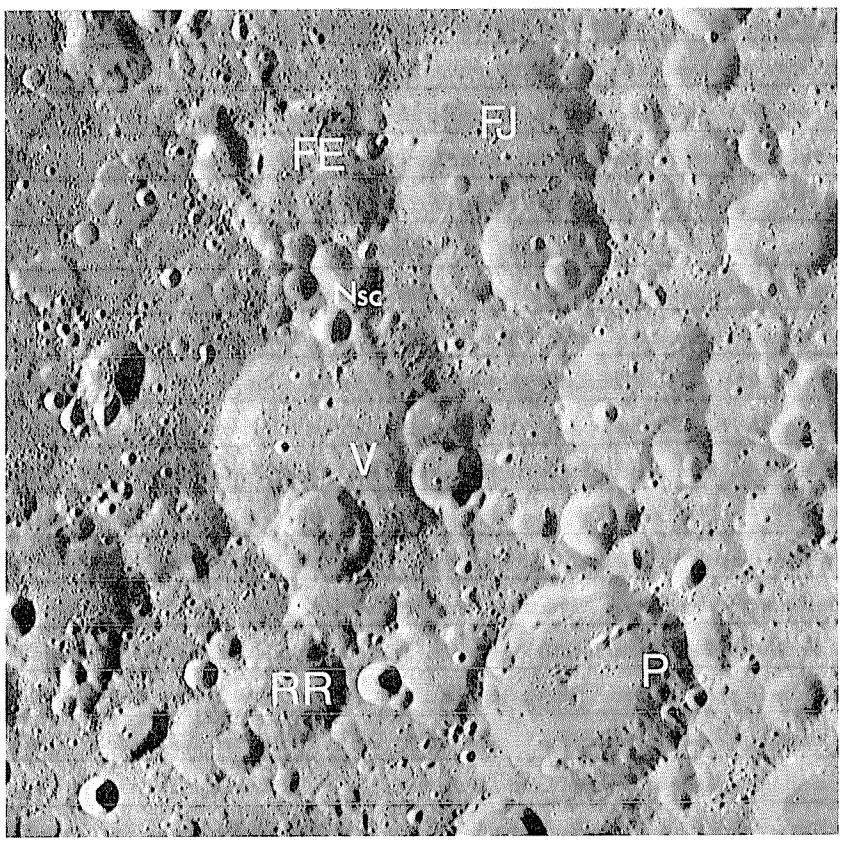

C

B. Poorly exposed pre-Nectarian deposits. Part of Vallis Rheita (VR), a secondary chain of Nectaris basin, overlain by Nectarian craters Rheita (R; 70 km, 37° S., 42° E.) and Young D (YD; 46 km). Other Nectaris-basin secondary chains (Nsc) are overlain by Nectarian primary crater Steinheil (S; 67 km). Crater Metius (M; 88 km) also is probably Nectarian because it interrupts pattern of Nectaris-basin deposits. Fabricius (F; 78 km) is much younger, probably Eratosthenian. Orbiter 4 frame H–71.

C. Moderately well exposed pre-Nectarian craters, including Vega (V; 76 km, 45° S., 63° E.), Fraunhofer E (FE; 42 km), Fraunhofer J (FJ; 63 km), Reimarus R (RR; 35 km), and Peirescius (P; 62 km), overlain by circular and subcircular Nectaris-basin secondary craters (Nsc). Vega and Peirescius are good type examples of pre-Nectarian crater morphology because large rim segments are preserved. Orbiter 4 frame H–52.

The well-dated basins of the four youngest age groups (table 8.2) have observable exterior deposits and secondary craters where well exposed and well photographed. The craterlike rims of Birkhoff and Lorentz are surrounded by ejecta and secondary craters to distances of at least one basin diameter (fig. 8.14). Secondary craters of Apollo are visible in the moderately well photographed zone south of the basin (fig. 8.15; Wilhelms and others, 1979), although they are covered by younger materials in the north and northeast. Apollo, Birkhoff, and the large crater or small basin Milne were considered to be Nectarian because of their evident ejecta (Wilhelms and El-Baz, 1977; Lucchitta, 1978; Wilhelms and others, 1979); the crater counts, however, indicate a pre-Nectarian age (as proposed for Apollo by Stuart-Alexander, 1978). Grimaldi ejecta appears to have smoothed its periphery, although it is too heavily obscured by Orientale deposits to demonstrate textured ejecta (figs. 4.3*I*, 4.4*H*; McCauley, 1973). The Planck and Schiller-Zucchius basins similarly lack textured ejecta but have smoothed the surrounding terrain and reduced the crater densities.

Freundlich-Sharonov is an especially instructive basin. The basin rings and interior are poorly photographed (fig. 4.3*P*), and their pattern emerged only upon mapping (Stuart-Alexander, 1978). Stuart-Alexander (1978) noted that superposed craters are relatively sparse in the surrounding terrain. A good photograph of the south basin periphery reveals relatively uncratered terrain lineate radially to the basin (fig. 8.7*A*). Analogy with Orientale indicates that the lineations are not tectonic or volcanic but were formed by the deposition of Freundlich-Sharonov ejecta. The basin would probably not have been discovered or interpreted as a typical impact basin without knowledge of other basins.

The progress of basin discovery suggests that additional pre-Nectarian basins will be found. Moreover, many basins probably formed before the South Pole-Aitken and Procellarum basins but are now completely obliterated. Basin deposits probably covered all parts of the Moon many times over in the manner displayed by the visible basins.

Craters

In the absence of reliable crater counts, morphologic comparisons are used to date stratigraphically isolated craters. These

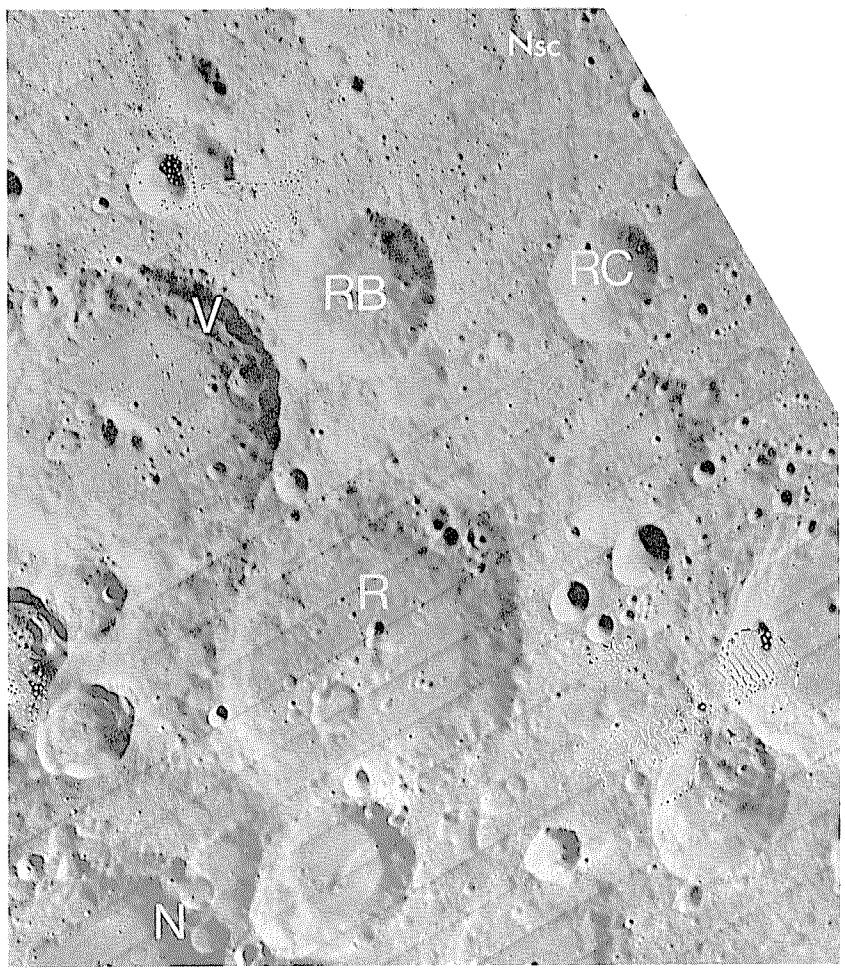

D. Well-exposed pre-Nectarian terrane, lightly pitted by Nectaris-basin secondary craters, affording additional typical pre-Nectarian morphologies. Subdued pits are superposed on pre-Nectarian craters Nearch (N; 76 km, 58.5° S., 39° E), Rosenberger (R; 96 km), Rosenberger C (RC; 47 km), Rosenberger B (RB; 33 km), and probably Vlacq (V; 89 km). Well-defined part of Nectaris-basin secondary field is in upper right (Nsc). Orbiter 4 frame H–83.

TABLE 8.2.—*Pre-Nectarian basins*

[Age groups in order of increasing age, each group arbitrarily headed by the largest basin of the group. Diameters from table 4.1. Parenthetical basins, existence not definitely established; parenthetical areas, buried; parenthetical densities, poor sample. Superposed craters are at least 20 km in diameter unless otherwise noted. Underlying and overlying basins determined from directly observed superpositional relations; n.d., no relations detected]

Age group	Basin	Diameter (km)	Superposed craters			Underlying basin		Overlying basin		Remarks
			Number	Area (10^6 km^2)	Density (craters/ 10^6 km^2)	Name	Figure	Name	Figure	
9	Apollo	505	57	0.480	119	(Grissom-White) South Pole-Aitken	8.15 9.21	Orientale, Hertzsprung, Korolev.	9.21	---
	Grimaldi	430	15	(0.154)	(97)	Procellarum	1.9	Orientale	1.9	---
8	Freundlich-Sharonov.	600	81	.629	129	Keeler-Heaviside	8.7	Moscoviense Mendeleev Korolev	8.7 --- 9.21	---
7	Birkhoff	330	50 (≥21 km)	.401	127	Lorentz, Coulomb-Sarton.	8.14	Imbrium Hertzsprung	8.14 8.14, 9.25	---
	Planck	325	9	.082	(110)	South Pole-Aitken Poincaré	1.3 1.5	Schrödinger	1.5	Small craters buried.
	Schiller-Zucchius.	325	16	(0.143)	(112)	n.d		Orientale Humorum	1.9, 7.6 9.24	Do.
	(Amundsen-Ganswindt).	355	11	(0.102)	(108)	South Pole-Aitken(?)	1.5	Schrödinger	1.5	Deeply buried.
6	Lorentz	360	33	.208	159	Coulomb-Sarton	8.14	Orientale, Imbrium Birkhoff	10.2 8.14	---
5	Smythii	840	74	.445	166	n.d		Crisium	1.5	---
	Coulomb-Sarton	530	43	(0.296)	(145)	n.d		Orientale, Imbrium, Hertzsprung, Birkhoff, Lorentz.	8.14	Small craters buried.
4	Keeler-Heaviside	780	69	.371	186	Ingenii(?) South Pole-Aitken	8.7 8.7	Mendeleev Freundlich-Sharonov	1.4 8.7	---
	Poincare	340	32	(0.168, partly)	(190)	South Pole-Aitken	1.5, 8.7	Schrödinger, Planck	1.5	Small craters buried.
	Ingenii	650	37 (≥22 km)	.228	162	South Pole-Aitken	8.7	Keeler-Heaviside(?)	8.7	Small craters obscured.
3	Lomonosov-Fleming.	620	63 (≥23 km)	.356	177	n.d		Imbrium, Crisium, Humboldtianum.	8.13	Do.
	Nubium	690	---	---	---	n.d		Imbrium Humorum	1.8, 8.10 8.10	Deeply buried.
	(Mutus-Vlacq)	700	80	.336	225	n.d		Imbrium, Nectaris	8.12	---
	Tranquillitatis	800	---	---	---	n.d		Imbrium Serenitatis Crisium Nectaris Fecunditatis	11.1 1.7, 5.17 --- 9.2, 11.1 ---	Deeply buried.
	Australe	880	129	(0.608, partly)	(>212)	South Pole-Aitken(?)	1.5	Schrödinger Nectaris	1.5 1.5, 9.5, 9.6	Complex burial pattern.
	Fecunditatis	990	---	---	---	Tranquillitatis	---	Crisium Nectaris	9.5 9.2	Deeply buried.
2	(Al-Khwarizmi/King)	590	63	.320	197	n.d		Smythii	8.11	---
	(Pingré-Hausen)	300	---	---	---	n.d		Orientale, Mendel-Rydberg.	1.9	---
	(Werner-Airy)	500	---	---	---	n.d		Imbrium, Nectaris	9.2	---
	(Balmer-Kapteyn)	550	---	---	---	n.d		Crisium, Nectaris	1.5	---
	(Flamsteed-Billy).	570	---	---	---	n.d		Orientale, Imbrium	8.10	---
	(Marginis)	580	---	---	---	n.d		Crisium, Humboldtianum.	9.4	---
	(Insularum)	600	---	---	---	Procellarum	8.10	Imbrium	8.10	---
	(Grissom-White)	600	---	---	---	South Pole-Aitken	8.15	Hertzsprung, Apollo	8.15	---
	(Tsiolkovskiy-Stark).	700	---	---	---	n.d		Milne Mendeleev	1.3 1.4	---
1	South Pole-Aitken.	2,500	---	---	---	n.d		Orientale, Mendel-Rydberg. Schrödinger, Planck, Poincare, Australe, (Sikorsky-Rittenhouse), (Amundsen-Ganswindt). Hertzsprung, Korolev, Apollo. Nectaris Keeler-Heaviside, Ingenii. Grissom-White)	1.9 1.5 9.21 9.6 8.7 8.15	---
	(Procellarum)	3,200	---	---	---	n.d		Most nearside basins.	8.10, 10.2	---

craters are compared with typical pre-Nectarian craters in the circum-Nectaris zone. Very few craters smaller than 20 km in diameter have been recognized as unequivocally pre-Nectarian because of severe degradation and the ambiguous significance of morphology (Wilhelms and others, 1978). In general, pre-Nectarian craters larger than 20 km in diameter that are degraded by the accumulated impact flux and not by catastrophic deposition of later deposits have lost fine-scale textures but still retain the overall shape of fresh craters (figs. 8.5*B–D*, 8.7*C*, 8.11, 8.14*B*, *C*; table 8.3). A short, sloping rim flank is still visible, but not the fine radial texture of the outer flanks that is displayed by younger craters; pre-Nectarian radial textures are visible only around basins, where they correspond to chains of secondary craters or, possibly, to large ridges of primary ejecta (fig. 8.7). The general morphology, but little sharp detail, of the crater rim-wall terraces is visible; the terraces are commonly amalgamated, and their edges cut by subradial notches. Floors are shallower, and rims more rounded, than in younger craters. Despite the degradation, many complete and well-defined rim segments are preserved. Because of this preservation of the overall morphology of the main impact sequence, even in older craters, good practice is to compare morphologies not only of the whole crater but also of small areas of the same size on each crater.

Like crater densities, morphologies of craters can be used as dating tools only if their geologic setting is also considered. Later deposits may degrade craters differentially (fig. 8.5). Moreover, typical "pre-Nectarian" morphologies may result from burial of a Nectarian crater by Nectarian or Imbrian basin deposits. For example, the subdued craters shown in figure 9.21 that are buried by deposits of the Nectarian Hertzsprung basin could be either Nectarian or pre-Nectarian. Much sharper, unburied craters could be pre-Nectarian (figs. 8.7*C*, 8.14*B*, *C*).

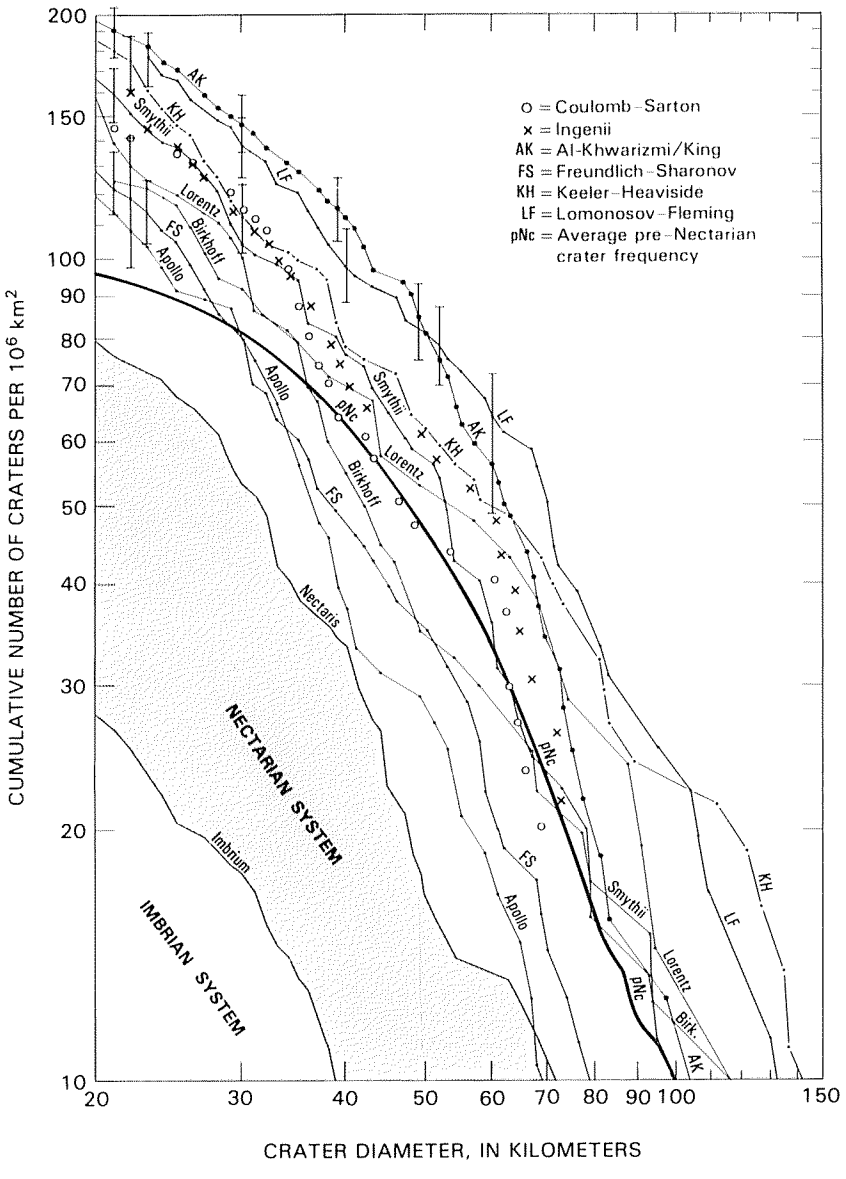

FIGURE 8.6.—Cumulative size-frequency distributions of craters at least 20 km in diameter superposed on pre-Nectarian basins. Materials of Nectarian and Imbrian Systems are indicated. Curve pNc (from Wilhelms and others, 1978) includes only pre-Nectarian craters, whereas each basin curve includes all postbasin primary craters of sizes indicated; curve pNc is average for best exposed pre-Nectarian terranes. Error bars represent square root of plotted point, added to and subtracted from value of point (compare table 8.2). Data tabulated in supplementary table.

TABLE 8.3.—*Representative pre-Nectarian craters*

[Cross rules divide table into craters smaller than 60 km, 60 to 119 km, and at least 120 km in diameter; interiors only are mapped in plate 6. F-S, Freundlich-Sharonov basin; N?, possibly Nectarian]

Crater	Diameter (km)	Center (lat)	Center (long)	Figure	Remarks
Daedalus U---------	30	4° S.	175° E.	8.7	Older than F-S.
Coriolis L---------	32	2° S.	173° E.	8.7	Younger than F-S.
Rosenberger B------	33	52° S.	46° E.	8.5	---
Reimarus R---------	35	48° S.	64° E.	8.5	Pitted by Nectaris basin.
Daedalus R---------	41	8° S.	75° E.	8.7	Older than F-S.
Fraunhofer E-------	42	43° S.	62° E.	8.5	Pitted by Nectaris basin.
Krusenstern--------	47	26° S.	6° E.	9.27	Mantled by Nectaris basin.
Rosenberger C------	47	52° S.	42° E.	8.5	---
Blanchinus---------	61	25° S.	31° E.	9.27	Mantled by Nectaris basin.
Peirescius---------	62	47° S.	68° E.	8.5	Typical.
Apianus------------	63	27° S.	8° E.	9.27	---
Fraunhofer J-------	63	42° S.	64° E.	8.5	Pitted by Nectaris basin.
Barbier------------	67	24° S.	158° E.	8.7	Relatively fresh.
Riccius------------	71	37° S.	27° E.	3.10D, 11.5	N?
Licetus------------	75	47° S.	7° E.	10.31	---
Nearch-------------	76	59° S.	39° E.	8.5	Typical.
Vega---------------	76	45° S.	63° E.	8.5	Do.
Birkhoff X---------	77	62° N.	150° W.	8.14	---
Mutus--------------	78	64° S.	30° E.	8.12	---
Esnault-Pelterie---	79	48° N.	141° W.	8.14	N?
Cyrano-------------	81	21° S.	158° E.	8.7	Relatively fresh.
Rabbi Levi---------	81	35° S.	24° E.	11.5	---
Zagut--------------	84	32° S.	22° E.	11.5	---
Vlacq--------------	89	53° S.	39° E.	8.5	---
Barrow-------------	93	71° N.	8° E.	10.15	N?
Playfair G---------	94	24° S.	7° E.	1.8, 9.27	---
Fra Mauro----------	95	6° S.	17° W.	2.5A, 10.19	N?; covered by the Fra Mauro and Cayley Formations.
Rosenberger--------	96	55° S.	43° E.	8.5	---
Schlesinger--------	97	47° N.	139° W.	8.14	---
Sacrobosco---------	98	24° S.	17° E.	7.9	Typical.
Purbach------------	118	26° S.	2° W.	1.8, 7.7	Do.
Goldschmidt--------	120	73° N.	3° W.	10.15	N?
Orontius-----------	122	40° S.	4° W.	1.8, 2.3	Typical.
Messala------------	124	39° N.	60° E.	9.3	---
Regiomontanus------	124	28° S.	1° W.	1.8, 7.7	---
Furnerius----------	125	36° S.	60° E.	9.5	Typical.
Stöfler------------	126	41° S.	6° E.	1.8, 10.31	---
Szilard------------	127	34° N.	106° E.	8.13	---
Paschen------------	133	14° S.	140° W.	9.21	---
Stebbins-----------	135	65° N.	143° W.	8.14	N?
Fowler-------------	136	43° N.	145° W.	8.14	---
Curie--------------	139	23° S.	92° E.	8.11, 10.46	---
Hirayama-----------	139	6° S.	94° E.	8.11	---
Lyot---------------	141	50° S.	84° E.	1.5, 10.46	---
Joliot-------------	143	26° N.	93° E.	4.7, 9.4, 9.28	---
Hipparchus---------	151	6° S.	5° E.	1.8, 3.10, 10.27	---
Ptolemaeus---------	153	9° S.	2° W.	1.8, 7.7, 10.28	---
W. Bond------------	158	65° N.	4° E.	1.7, 10.6, 10.15	---
Richardson---------	161	31° N.	100° E.	8.13	---
Heaviside----------	163	11° S.	167° E.	1.4, 8.7	---
Maginus------------	163	50° S.	6° W.	4.6A	Typical.
Einstein-----------	170	17° N.	89° W.	3.9A	---
Tsander------------	171	6° N.	149° W.	9.21	---
Fabry--------------	179	43° N.	101° E.	1.2	---
Von Kármán---------	179	44° S.	176° E.	8.15	---
Janssen------------	190	45° S.	42° E.	3.10D, 9.1, 9.2	Covered by the Janssen Formation.
Galois-------------	207	14° S.	152° W.	9.21	---
Landau-------------	221	43° N.	119° W.	4.2F, 8.14	---
Campbell-----------	225	45° N.	153° E.	4.2G, 12.9	---
Von Kármán M-------	225	47° S.	176° E.	8.15	---
Schickard----------	227	44° S.	55° W.	1.9, 7.6	---
Deslandres---------	234	33° S.	5° W.	1.8	Typical.
Pasteur------------	235	11° S.	105° E.	1.2, 8.11	Do.
Leibnitz-----------	236	38° S.	179° E.	8.15	---
Fermi--------------	238	20° S.	123° E.	1.3	---
Milne--------------	262	31° S.	113° E.	1.3, 4.2J, 8.11	Ring arcs.
Gagarin------------	272	20° S.	149° E.	1.4, 3.5, 4.2K	Typical.

Despite the problems, the results of dating basins by superpositional relations, crater counts, and assessments of superposed crater morphology are generally consistent. No known craters with pre-Nectarian morphology are clearly superposed on Nectarian basins. This general internal consistency is the outcome of a series of iterations in which the morphologic criteria for pre-Nectarian age were repeatedly reassessed. Anomalous rebound of craters inside basins and anomalous degradation by deposits of younger craters were detected by geologic mapping. Thus, some assignments of crater age in this volume differ from those shown on earlier geologic maps, including those by Wilhelms and El-Baz (1977) and Wilhelms and others (1979). Pre-Nectarian craters are subdivided on the paleogeologic map (pl. 6) as exposed (solid black), buried (solid rim-crest outline), or possibly Nectarian (dashed rim-crest outline).

A total of 1,208 pre-Nectarian craters larger than 30 km in diameter, 456 of which are unburied by pre-Nectarian or younger deposits, are mapped here (pl. 6). They vary greatly in areal density because the units that underlie them vary in age and because the thickness of overlying deposits affects the number of buried craters

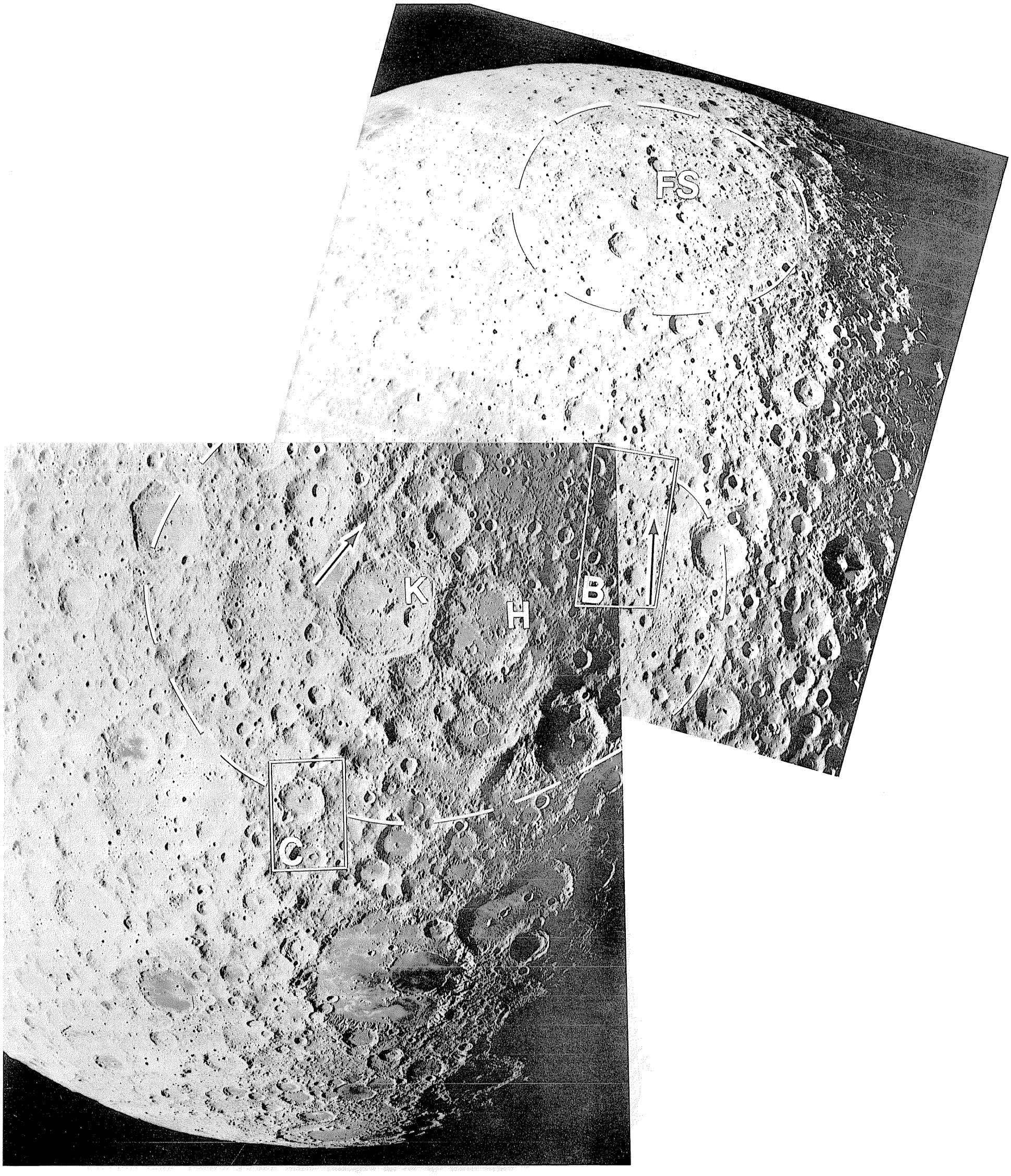

FIGURE 8.7.—Stratigraphic relations between pre-Nectarian units on farside.

A. Radial lineations (arrows) of Freundlich-Sharonov basin (FS), superposed on Keeler-Heaviside basin (named for unrelated craters Keeler [K; 169 km, 10° S., 162° E., probably Lower Imbrian] and Heaviside [H; 163 km, pre-Nectarian]; compare figs. 4.3*P, S*); areas of *B* and *C* are outlined. Orbiter 2 frames M–75 (lower left) and M–34 (upper right); overlaps figure 1.4.

that can still be seen. A density of 77 unburied pre-Nectarian craters per million square kilometers (422 craters min 30 km diam in 5.45×10^6 km^2) was determined for terrain of the oldest basins (age groups 1–5, table 8.2) and other heavily cratered terrain. The younger pre-Nectarian basins (age groups 6–9) display a much lower average density of 10 such craters (34 in 3.24×10^6 km^2). Extrapolation of the larger value to the whole Moon (area, 38×10^6 km^2) suggests that a minimum of 2,940 craters larger than 30 km in diameter formed during pre-Nectarian time. Assuming that their deposits were as extensive relative to crater size as are those of young craters, the deposits covered about 110 percent of the Moon's surface area. Based on the Nectarian frequency (see chap. 9), which is less affected by saturation, the actual number of pre-Nectarian craters of this size that formed while the 28 pre-Nectarian basins of groups 2 through 9 were forming was closer to 3,400. A still greater, unknown number formed earlier.

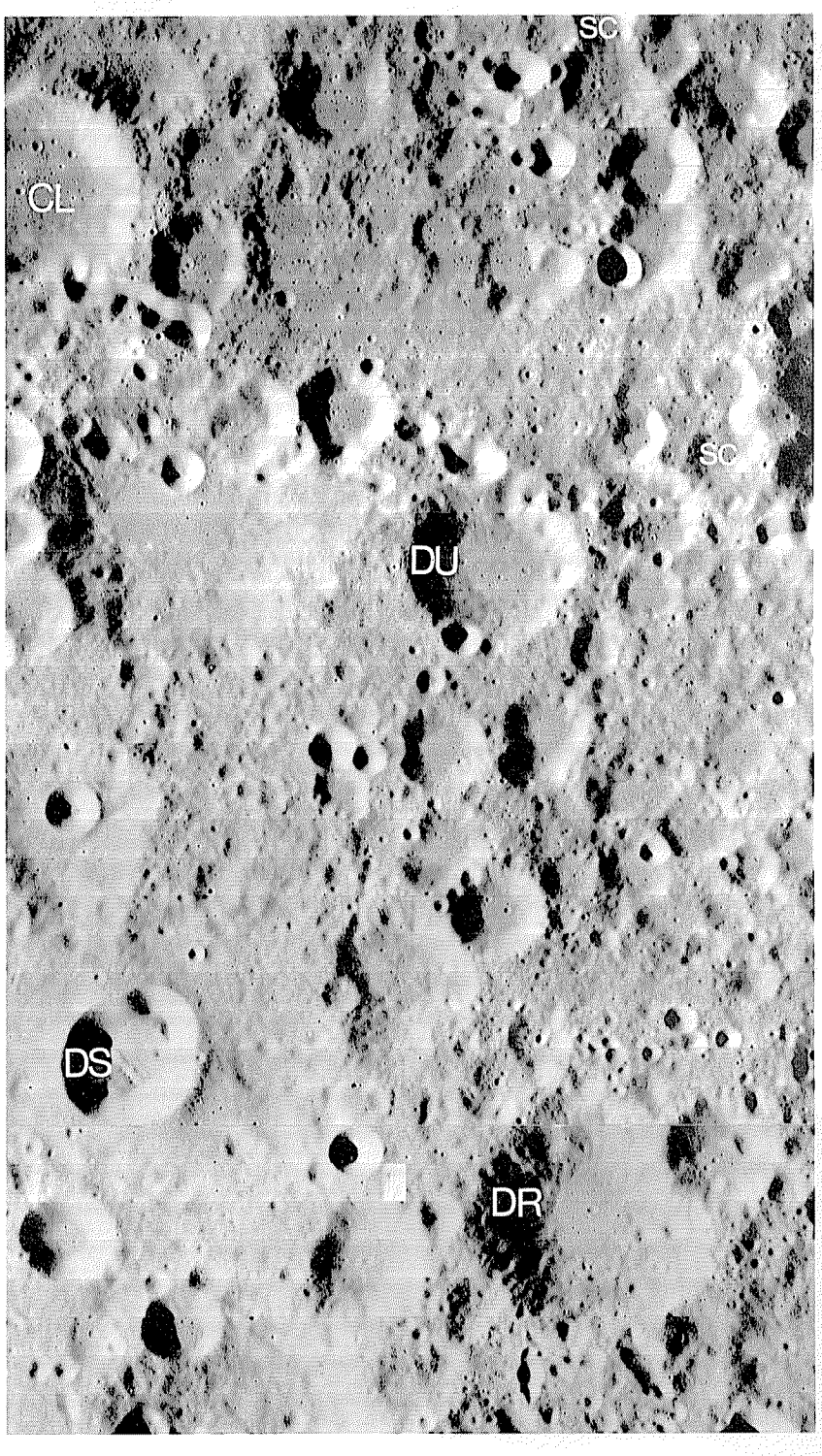

B. Pre-Nectarian terrane pitted by probable secondary craters of Freundlich-Sharonov basin (sc) and other, smaller secondaries. Craters older than Freundlich-Sharonov include Daedalus R (DR; 41 km) and Daedalus U (DU; 30 km); Coriolis L (CL; 32 km) may be younger. A much younger crater chain secondary to a distant impact crater or basin, probably Orientale (centered 2,800 km to east), is also superposed on Coriolis L and Daedalus U. Crater Daedalus S (DS; 20 km) is also young, probably Imbrian. Orbiter 2 frame H–33.

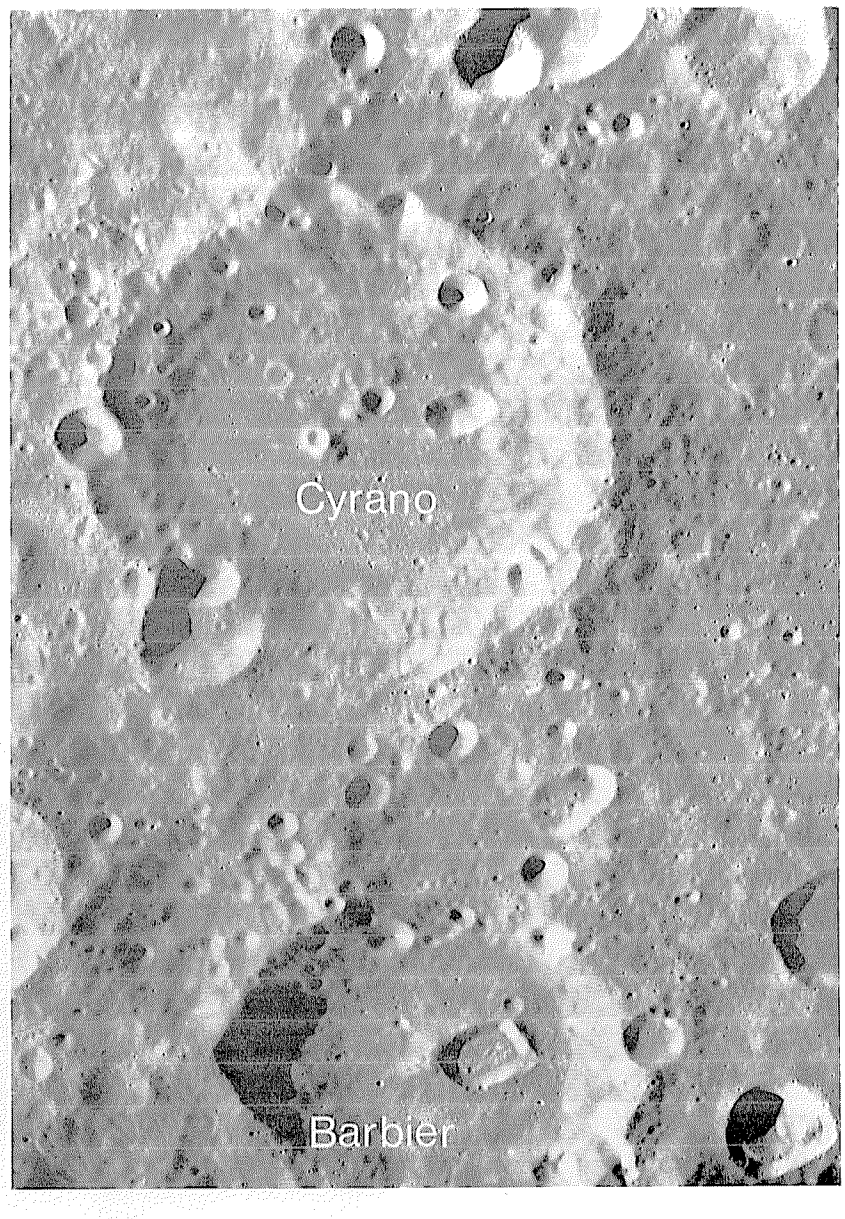

C. Craters Cyrano (81 km) and Barbier (67 km), similar to pre-Nectarian craters in figure 8.5 and of a morphologic type absent in *B*, are beyond range of Freundlich-Sharonov deposits; thus, Cyrano and Barbier are probably pre-Nectarian and possibly older than Freundlich-Sharonov basin, despite moderately sharp topography. Orbiter 2 frame H–75.

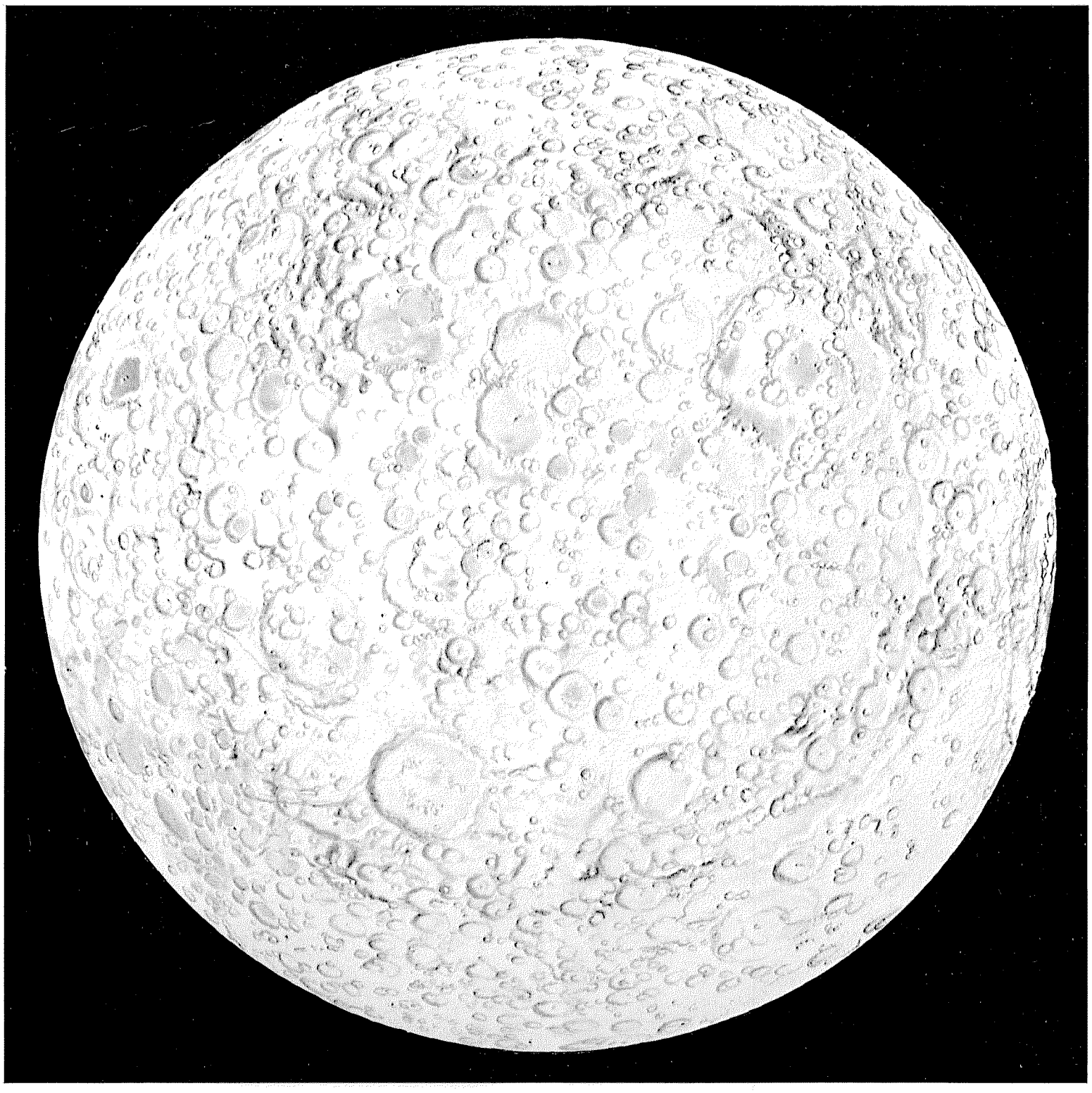

FIGURE 8.8.—Pre-Nectarian South Pole-Aitken basin, centered around lat 56° S., long 180°. Airbrush drawing by Donald E. Davis, courtesy of the artist.

FIGURE 8.9.—South Pole-Aitken massifs photographed by Apollo 8. Arrow indicates crater Mohorovičić A (20 km, 16° S., 163° W.) atop one arcuate massif; other massifs along lat 22° S. occupy horizon. At time of Apollo 8 mission, relation of the large mountains to a basin had not yet been recognized. View southeastward. Apollo 8 frame H–2319.

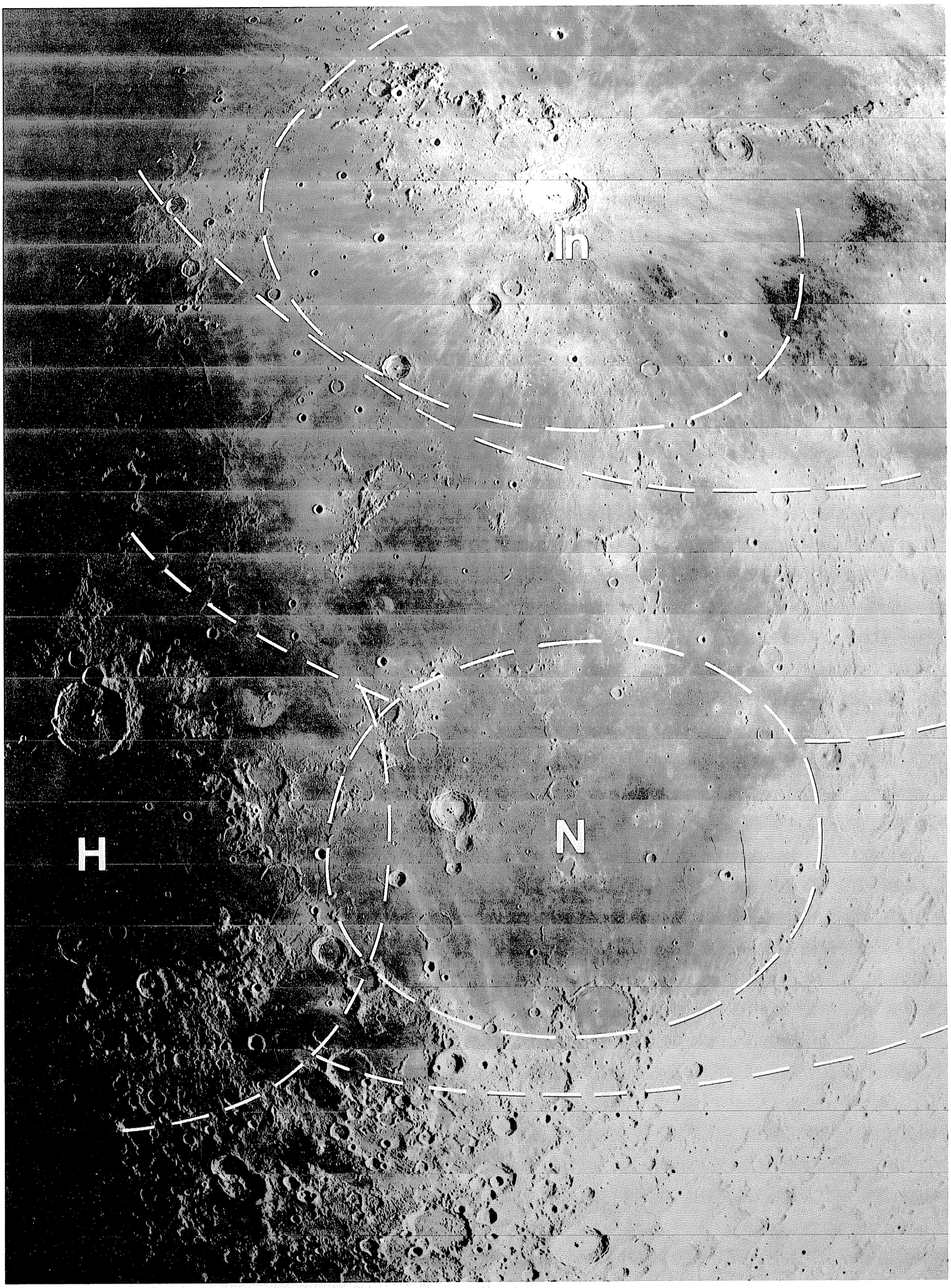

FIGURE 8.10.—Part of southern Oceanus Procellarum region, including Nectarian Humorum basin (H), pre-Nectarian Insularum (In) and Nubium (N) basins, and three rings of pre-Nectarian Procellarum basin (Whitaker, 1981); central Procellarum ring is expressed here mostly by mare ridges (compare fig. 5.26). Shallowness of mare is indicated by many islands belonging to basins and craters that are superposed on Procellarum basin (pl. 3). Orbiter 4 frame M–125.

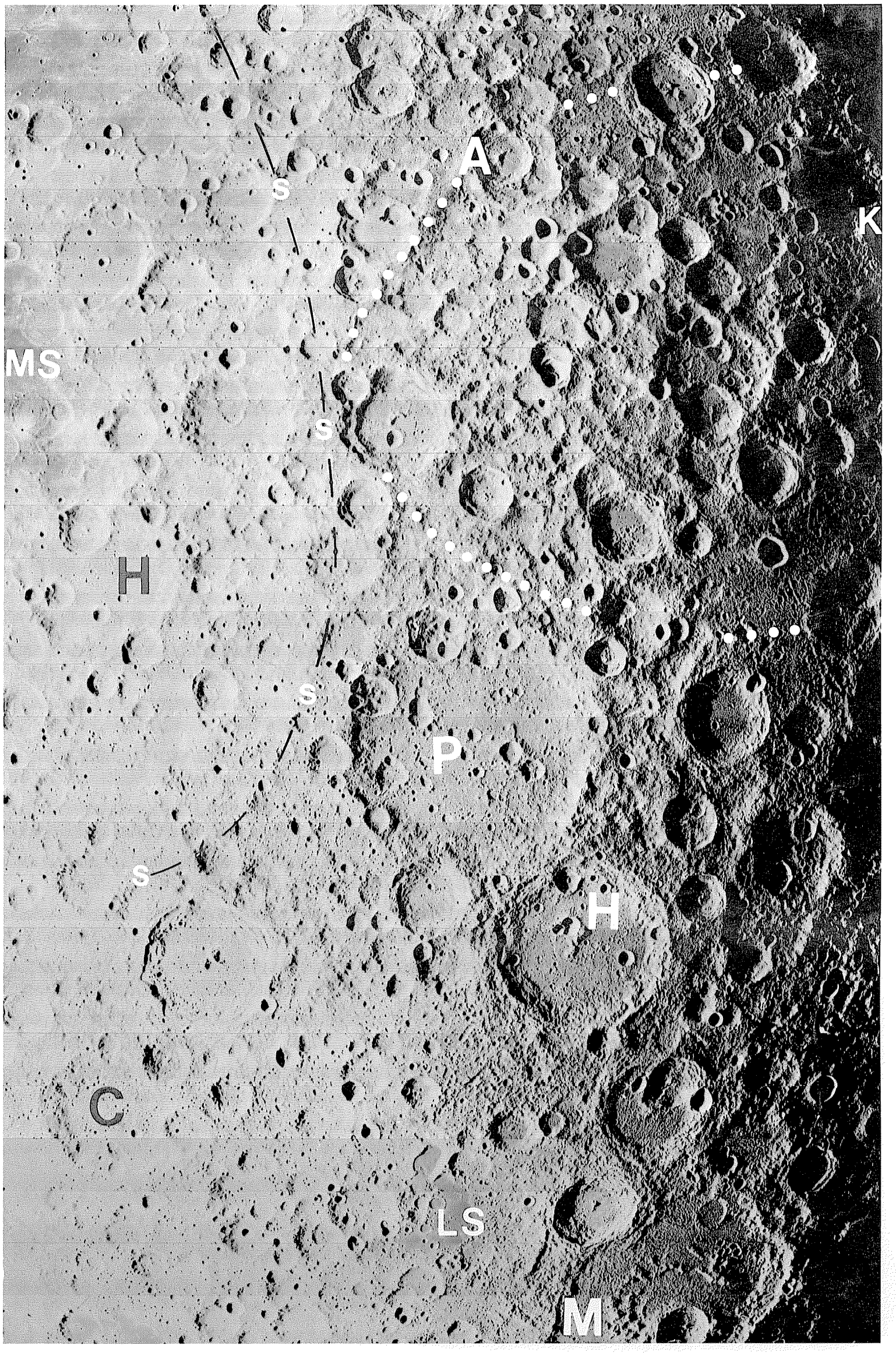

FIGURE 8.11.—Large section of western farside, centered on craters Pasteur (P; 235 km, 12° S., 105° E., Pre-Nectarian) and Hilbert (H; 170 km, 18° S., 108° E., Nectarian), both filled by cratered plains. White dots, indefinite pre-Nectarian basin Al-Khwarizmi/King (Wilhelms and El-Baz, 1977), named for craters Al-Khwarizmi (A; 65 km, 7° N., 107° E., Nectarian) and King (K; 77 km, 5° N., 121° E., Copernican); most conspicuous part of rim is southwest of letter A. MS, Mare Smythii; s and black dashes, rim of pre-Nectarian Smythii basin. Lacus Solitudinis (LS) is not related to known basins. Pre-Nectarian crater or small basin Milne (M; 265 km, 31° S., 113° E.) has basinlike ring structure but is omitted from table 4.1 because of its size. Orbiter 2 frame M–196.

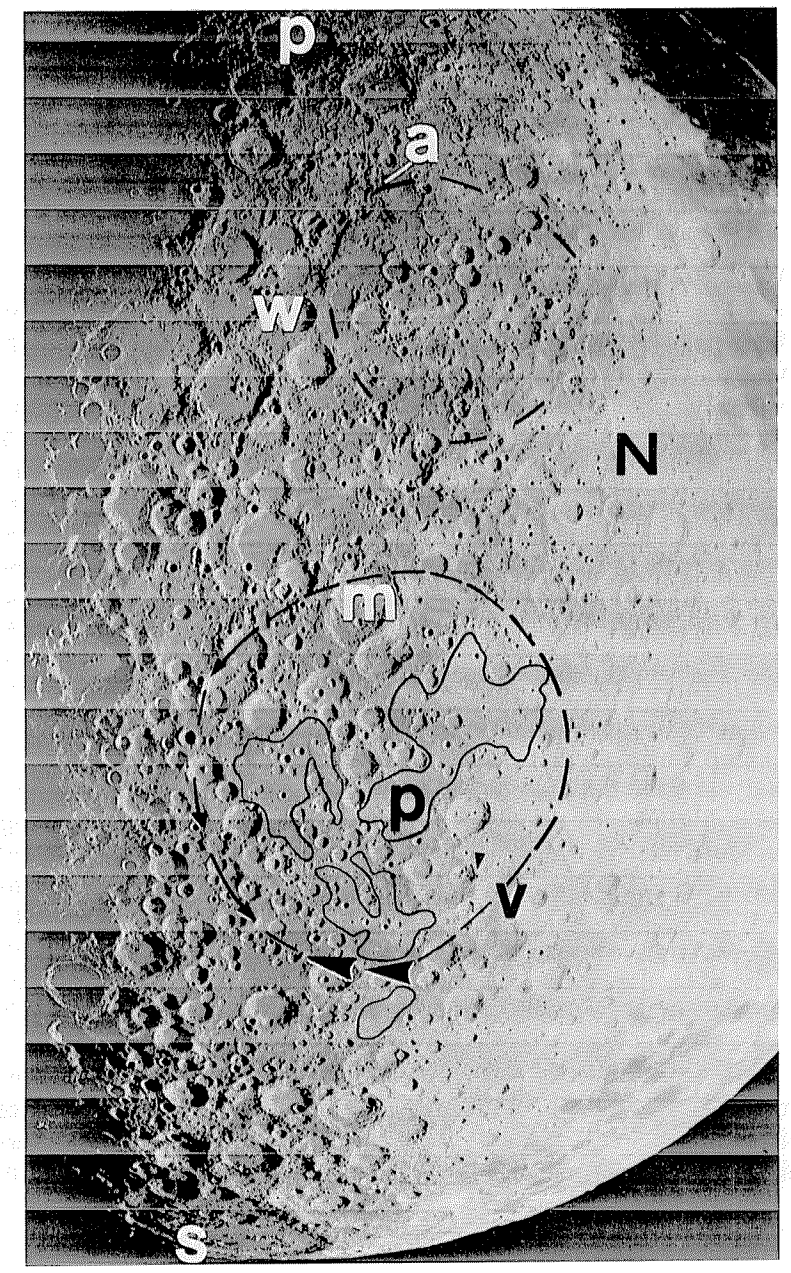

A

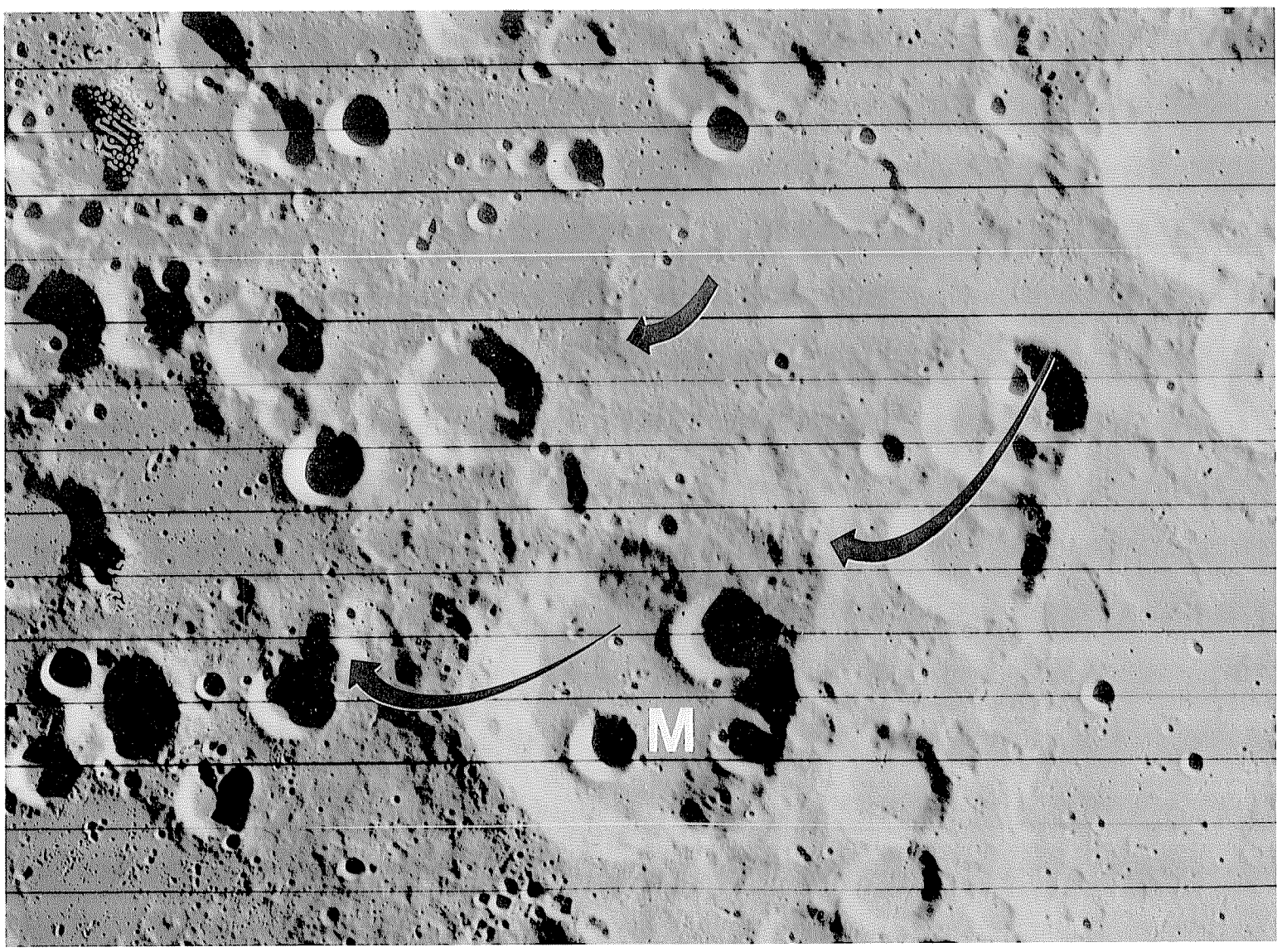

B

FIGURE 8.12.—Pre-Nectarian Mutus-Vlacq and Werner-Airy basins.

A. South-central nearside and area around south pole including Imbrian Schrödinger basin on farside (s; 320 km, 76° S., 134° E.). Black dashes, rims of Mutus-Vlacq (below) and Werner-Airy (indistinct, above). Arrowheads, prominent massifs of Mutus-Vlacq; those indicated by larger arrowheads are also shown in *B*. Black p, Nectarian plains concentrated in Mutus-Vlacq basin. N, Nectaris-basin rim (Rupes Altai). Pre-Nectarian craters include Ptolemaeus (white p; 153 km, 9° S., 2° W.) and Vlacq, (v; 89 km, 53.5° S., 39° E.); Nectarian craters include Maurolycus (m; 114 km, 42° S., 14° E.) and Airy (a; 37 km, 18° S., 5.5° E., possibly Imbrium-basin secondary crater); Werner (w; 70 km, 28° S., 3.5° E.) is Eratosthenian. Orbiter 4 frame M–95.

B. Detail of Mutus-Vlacq massifs. Large arrows indicate same massifs as large arrowheads in *A*. Small arrow indicates hill possibly belonging to an inner ring. M, Mutus (78 km, 63.5° S., 30° E., pre-Nectarian). Orbiter 4 frame H–82.

VOLCANIC ROCKS

The discovery of ancient volcanic rocks on the Moon would be of great interest from the standpoints of both petrogenesis and stratigraphy. The unforewarned geologist might think that such rocks have been found in abundance because the terms "highland basalt," "KREEP basalt," and numerous other "basalts" are so common in the literature. However, no pristine samples of terra composition are known to be both pre-Nectarian in age and volcanic in origin; volcanic KREEP basalt of Early Imbrian age is the oldest currently recognized terra-type volcanic material (see chap. 10). Fragments of mare basalt have been recovered from breccia deposits emplaced in the Nectarian and Imbrian Periods, and a few have been radiometrically dated (table 9.5; chaps. 9, 10). Whether they are pre-Nectarian depends on the absolute age of the Nectaris basin (see chap. 9); none are of definite pre-Nectarian age.

Moreover, no plains or other terrane of pre-Nectarian age sufficiently resemble maria to be definitely established as volcanic. Plains in such basins as Mutus-Vlacq (fig. 8.12) may consist of pre-Nectarian basalt underlying Nectarian ejecta, but this is uncertain (see chap. 9). All pre-Nectarian interbasin terrane is ascribable to basin deposits and is here mapped accordingly (pl. 6).

Despite the absence of firm evidence for pre-Nectarian volcanism, mare and KREEP basalt may have been extruded during the period. The extensive early plutonism suggests accompanying volcanism, and some of the recovered mare-basalt clasts are, at least, very close to pre-Nectarian in age. Another line of indirect evidence for volcanism is the concentration of KREEP revealed by gamma-ray spectrometers in the Imbrium-Procellarum region. The Procellarum basin may have unroofed deep-seated KREEP-rich material that was then excavated by further impacts; alternatively, however, KREEP basalt may actually have been extruded volcanically into the basin (fig. 8.4*B*; Wood, 1972b; Cadogan, 1974, 1981). These pre-Nectarian extrusions could have been recycled by later impacts and mare extrusions, so that the KREEP chemistry appears to be concentrated today in deposits of Archimedes, Aristarchus, Copernicus, and other craters in the region. Continued sampling might well disclose pre-Nectarian volcanic rocks here and elsewhere on the Moon.

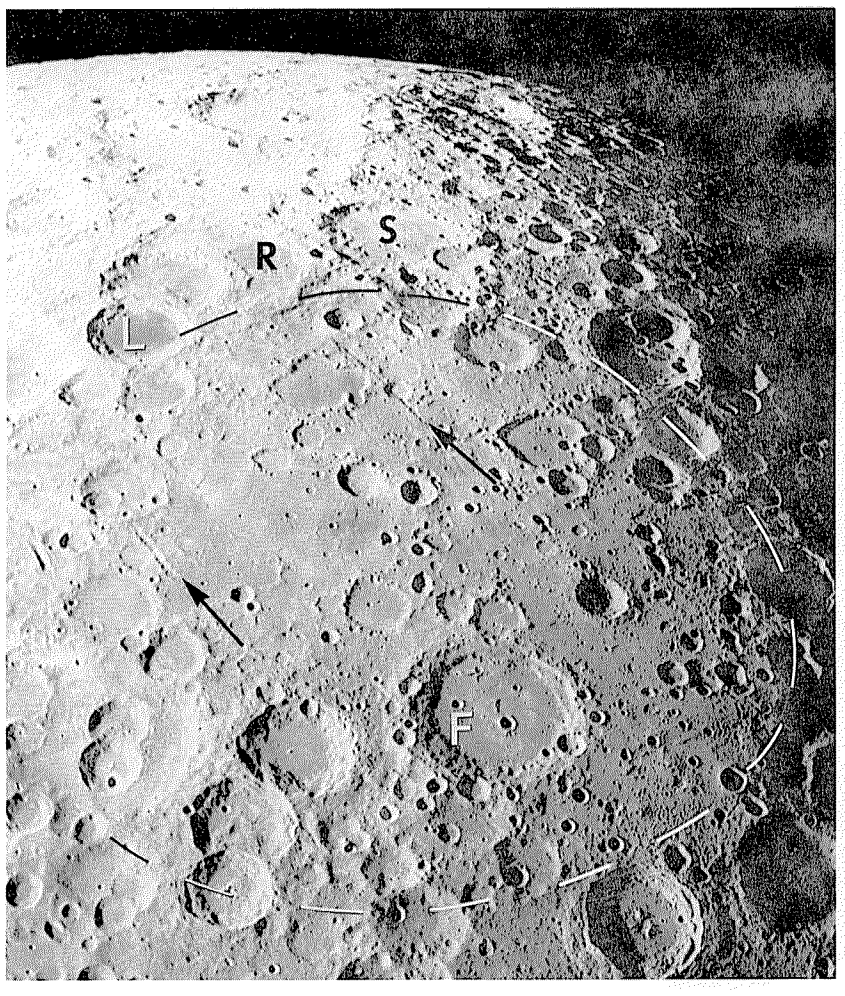

FIGURE 8.13.—Pre-Nectarian Lomonosov-Fleming basin (dashes outline rim), named for unrelated craters Fleming (F; 130 km, 15° N., 109.5° E., Nectarian) and mare-filled Lomonosov (L; 93 km, 27.5° N., 98° E., Lower Imbrian). Pre-Nectarian craters include Richardson (R; 161 km) and Szilard (S; 127 km). Nectarian and Imbrian plains occupy much of basin interior, especially between arrows and east of Fleming. Groovelike crater chains (arrows; above, Catena Artamonov; below, Catena Dziewulski) are radial to and, probably, secondary to the Imbrium basin, centered 3,000 km away on opposite side of Moon. Apollo 12 frame H–8296.

CHRONOLOGY

The earliest pre-Nectarian event was the origin of the Moon. Before the space age, the Moon's age was inferred from U-Th-Pb ages of the Earth and meteorites to be 4.55 ± 0.07 aeons, assuming that all these bodies formed contemporaneously (Patterson, 1956). Absolute dating of lunar rocks based on radiometric ages and assumed initial isotopic ratios (model ages) is consistent with 4.55 aeons ago as the approximate time of lunar origin (Tatsumoto and others, 1973, 1977; Tera and Wasserburg, 1974; Nyquist, 1977; Tilton and Chen, 1979).

Some recovered clasts of ANT rock yield very old isotopic ages (table 8.4). Ferroan anorthosite is difficult to date because it contains very little Rb, Nd, and Sm; its low initial $^{87}Sr/^{86}Sr$ ratios are consistent with, but do not require, very primitive ages (Papanastassiou and Wasserburg, 1975, p. 1483; Tatsumoto and others, 1977). More precise ages appearing to be crystallization ages have been obtained for pristine Mg-suite rocks (table 8.4). They range as old as 4.51 ± 0.07 aeons for inclusions in olivine of troctolite sample 76535 from the Apollo 17 landing site (Papanastassiou and Wasserburg, 1976). The analysts were uneasy about the similarity of this age to that of the Moon, but the age may, indeed, have been set by igneous melting in the Moon shortly after its accretion (Carlson and Lugmair, 1981b). A later event in the same rock's history at about 4.26 aeons ago is recorded by Sm-Nd mineral isochrons and ^{40}Ar-^{39}Ar plateaus. If the 4.51-aeon age is an artifact, this later age may date the crystallization of the troctolite, or it may date the end of a long cooling episode during which isotopic reequilibration was possible (Gooley and others, 1974; Lugmair and others, 1976; Carlson and Lugmair, 1981b).

Interpretation of such internal isochrons as dates of igneous melting, along with evidence for very early geochemical fractionations (Rb-Sr, Pb-U, Sm-Nd), leads to the conclusion that the differentiation which formed the lunar crust began during or immediately after accretion (for example, Papanastassiou and Wasserburg, 1971a, 1975, 1976; Tera and Wasserburg, 1974; Lugmair and others, 1975; Nunes and others, 1975; Herbert and others, 1977; Nyquist, 1977; Tatsumoto and others, 1977; Lugmair and Carlson, 1978; Carlson and Lugmair, 1981a, b). How long this differentiation lasted and the extent of igneous activity after crustal formation but before extrusion of the visible mare basalt are unanswered questions. The geologically important date of when the crust solidifed enough to support basin-and-crater topography probably is between 4.4 and 4.2 aeons ago; the

TABLE 8.4.—*Radiometric ages of samples of pristine pre-Nectarian lunar rocks*

[Sample 15455, Apollo 15 (Ryder and Bower, 1976); numbers beginning with 6, Apollo 16 (Ulrich and others, 1981); numbers beginning with 7, Apollo 17 (Wolfe and others, 1981). Numbers after commas represent splits of sample. Mineralogy: cpx, clinopyroxene; ol, olivine; opx, orthopyroxene; pl, plagioclase.
Ages calculated using decay constants recommended by the International Union of Geological Sciences (IUGS) (Steiger and Jäger, 1977).
References: B75, Bogard and others (1975); CL81a, Carlson and Lugmair (1981a); CL81b, Carlson and Lugmair (1981b); C75, Compston and others (1975); HS75, Husain and Schaefer (1975); HW75, Huneke and Wasserburg (1975); J77a, Jessberger and others (1977a); L75, Leich and others (1975); L76, Lugmair and others (1976); N76, Nakamura and others (1976); N79b, Nyquist and others (1979b); N81a, Nyquist and others (1981a); PW75, Papanastassiou and Wasserburg (1975); PW76, Papanastassiou and Wasserburg (1976); S74, Stettler and others (1974)]

Sample	Source rock and lithology (minerals in volume percent)	Age (aeons)	Method	Reference	Remarks
15455	Norite clast (60-65 pl, 35-40 opx) from black-and-white breccia.	4.48±0.12	Rb-Sr	N79b	Isotopic systems disturbed (CL81b).
67435	Tiny plagioclase clasts from 354-g polymict breccia.	4.35±0.05	Ar-Ar	J77a	---
67667	7.9-g rake sample of lherzolite (58 ol, 21 pl, 15 opx, 5 cpx).	4.18±0.07	Sm-Nd	CL81a	Crystallization or impact-excavation age.
72255	Plagioclase from 2-cm "Civet Cat" norite clast from boulder 1, station 2.	3.93±0.03 4.08±0.05	Ar-Ar Rr-Sr	L75 C75	Possibly as old as 4.36±0.13 aeons (C75).
72417	Dunite (93 ol); part of clast 72415-72418 from boulder 3, station 2.	4.45±0.10	Rb-Sr	PW75	Imprecise whole-rock isochrons.
73255, 27,45	Granulated 0.9-g norite clast (53 pl, 40 opx) from 394-g polymict breccia 73255.	4.23±0.05	Sm-Nd	CL81b	Crystallization age; not disturbed.
76535	156-g rake sample of troctolite (37-60 ol, 35-58 pl, 4-5 opx).	4.16±0.04 4.26±0.02 4.26±0.06 4.27±0.08 4.51±0.07	Ar-Ar Ar-Ar Sm-Nd Ar-Ar Rb-Sr	HW75 HS75 L76 B75 PW76	Crystallization or impact-excavation age. Do. Do. Do. Crystallization age or artifact.
77215, 37	Norite clast from station 7 boulder.	3.98±0.04 4.33±0.04 4.37±0.07	Ar-Ar Rb-Sr Sm-Nd	S74 N76 N76	Crystallization age at least 4.33 aeons (CL81b).
78236	Shocked norite clast (opx>pl) from station 8 boulder.	4.34±0.05 4.38±0.02 4.39 4.43±0.05	Sm-Nd Rb-Sr Ar-Ar Sm-Nd	CL81b N81a N81a N81a	Crystallization age is probably close to 4.34 aeons (CL81b).

older date is more common in the literature (for example, Tera and Wasserburg, 1974). Taylor (1982, p. 246), however, suggested that crystallization proceeded rapidly until 4.3 aeons ago and that intense impact bombardment kept the crust thoroughly mixed and chemically requilibrated until about 4.2 aeons ago. The picture of igneous petrogenesis that is emerging furthermore suggests that the differentiation was complex. Local zones may have solidified early, especially near the surface, and local hotspots probably persisted until late. Early-formed crust was probably intruded by later plutons, dikes, and sills. This complex, late-ending history (Nunes and others, 1975; Nakamura and Tatsumoto, 1977, p. 2312; Carlson and Lugmair, 1981b) seems more likely than the simpler scenarios that appear in much of the literature.

Some pre-Nectarian clasts record probable postcrystallization impacts. The 4.26-aeon event in the history of troctolite sample 76535 may have been an impact that ended the cooling (Papanastassiou and Wasserburg, 1976; Carlson and Lugmair, 1981b). Dunite sample 72415–72418 was shocked at least once, probably during the pre-Nectarian, before incorporation into the Apollo 17 melt-rich breccia deposits (Dymek and others, 1975). The more abundant Apollo 17 norite samples were also shocked before final emplacement (Nakamura and Tatsumoto, 1977; see summary by James, 1980). The shock events may have been the formation of one of the pre-Nectarian basins in the Serenitatis target area, such as Tranquillitatis (pl. 6). Similarly complex, extended histories have been detected in other primitive lunar rocks (table 8.4). The later events indicate that the isochrons have been disturbed, and so the pristine ages are not accurate except as minima.

The impact processing manifest in samples from younger deposits generally supports the high early impact rate indicated by the abundance of observed pre-Nectarian basins and craters. For example, widespread thermal metamorphism at shallow depths, probably caused by accumulation of hot ejecta blankets, is suggested as the origin of the granulitic textures of many impact-mixed rocks (Warner and others, 1977; Bickel and Warner, 1978; James, 1980). However, more specific information about pre-Nectarian chronology applicable to the stratigraphic record has not been forthcoming from the rocks. Attempts to calibrate the impact flux by means of the amounts of siderophile elements or impact-melt rock are hindered by uncertainties about projectile-to-ejecta ratio or energy partitioning between impact melt and excavation (for example, Lange and Ahrens, 1979).

Another potential method of establishing the emplacement ages of pre-Nectarian units is the classic one of calibrating crater frequencies with absolute ages. However, the relative ages of ancient surfaces are difficult to determine precisely by crater frequencies because they are saturated to large crater diameters (Baldwin, 1969; Hartmann, 1975); all the frequency curves will have similar intercepts at 20-km diameter and will differ only by subtle differences in the steady-state diameters. In figure 8.16, an envelope of curves is fitted to (1) the approximately known relative ages and well known absolute ages of the Imbrian and Eratosthenian mare-basalt samples (see chaps. 11, 12), (2) the well known relative and absolute ages (3.85 aeons) of the Imbrium basin (chap. 10), (3) the well known relative age and the estimated absolute age (3.92 aeons) of the Nectaris basin (chap. 9), and (4) the highest crater frequency found in this study, that within the limits of the possible Al-Khwarizmi/King basin. The boxes for the Imbrium, Nectaris, and Al-Khwarizmi/King surfaces are bounded below by the actual observed cumulative frequencies of all craters larger than 20 km in diameter and above by projections to 20-km diameter from the parts of the curves representing craters large enough to have escaped steady-state obliteration (fig. 8.6). Proper comparison of the boxes requires comparing the same edge of each. This extrapolation suggests that the Al-Khwarizmi/King crater population is between 3.97 and 4.03 aeons old and that, accordingly, the basin itself, part of pre-Nectarian group 2, is equally old or somewhat older.

A steep exponential decline like that plotted in figure 8.16 is only one of many possible models of the early impact rate (Hartmann, 1965a, 1966, 1972c; Baldwin, 1971; Shoemaker, 1972, 1981; Wetherill, 1975a, 1977a, b, 1981; Basaltic Volcanism Study Project, 1981, chap. 8). Possibly, the pre-Nectarian impact rate was closer to the Nectarian rate (19,000 craters and 157 basins per aeon; see chap. 9) than is generally assumed. In this case and if, additionally, the pre-Nectarian crater size-frequency distribution was originally the same as the Nectarian (small craters not yet destroyed), 3,400 craters from 30 to 300 km in diameter, as well as the 28 basins of pre-Nectarian groups 2 through 9, formed from 4.1 to 3.92 aeons ago. A similar figure of 4.06 aeons for the age of the oldest group-2 basins is derived by assuming a constant rate of surface blanketing by basin deposits (Nectarian basin deposits one basin diameter in radius theoretically cover 41 percent of the Moon, and group 2–9 pre-Nectarian deposits cover 84 percent). Thus, the models of steeply declining and constant impact rates bracket the age of the oldest group-2 basins and accompanying craters between about 4.1 and 4.0 aeons. The younger age is more likely if the early impact rate declined as steeply as shown in figure 8.16, and may even be too old if the impacts declined still more steeply. On the other hand, 4.1 aeons may be too young if the Nectarian Period lasted longer than 0.07 aeon. I tentatively adopt 4.1 aeons as the age of the oldest group-2 basins because of this intermediate position among the likely estimates.

The two giant basins of group 1, Procellarum and South Pole-Aitken, probably formed before all the other visible basins and all the visible craters. Because these basins are probably saturated by impact structures of basin size, their ages are very difficult to estimate without more calibration points or better models of the impact rate than are available. The two models of the impact rate discussed here imply different scenarios in the early era when these basins formed. If the impacts declined steeply all through pre-Nectarian time, far more basins formed than are observed. This scenario is, in fact, consistent with the extreme impact processing observed in the lunar crustal rocks and the relative paucity of "pristine" samples. If extrapolated to the early pre-Nectarian, however, such steep curves also imply that an unrealistically great mass of material impacted the Moon since its accretion (R.B. Baldwin, oral commun., 1983). This difficulty is avoided if basins formed throughout pre-Nectarian and Nectarian time at an approximately constant rate. About 14 basins in addition to the two giant basins would then have formed from 4.2 to 4.1 aeons ago—still enough for considerable impact processing of the crust.

In summary, the many uncertainties preclude accurate estimates of any pre-Nectarian event after the origin of the Moon 4.55 aeons ago. The many great impacts that must have preceded 4.2 aeons may have struck either a solid or a mushy crust; the geologic record does not specify which, but frequencies of craters and basins are, at least, consistent with the 4.2-aeon date of crustal solidification given earlier. Procellarum, South Pole-Aitken, and at least 14 now-obliterated basins formed between crustal solidification and the oldest of the 28 pre-Nectarian basins of groups 2 through 9. The group-2 basins began about forming 4.1 aeons ago if the Nectarian Period lasted 0.07 aeon (from 3.92 to 3.85 aeons ago) and if the impact rate was approximately constant during pre-Nectarian and Nectarian time. These conservative estimates of 4.2, 4.1, and 3.92 aeons for the major milestones of the pre-Nectarian period are consistent with available data but may be considerably altered by better data on the age of the Nectaris basin or the early impact rate. At least, pre-Nectarian basins and craters clearly formed in such abundance that they repeatedly destroyed earlier features and reworked earlier crustal materials.

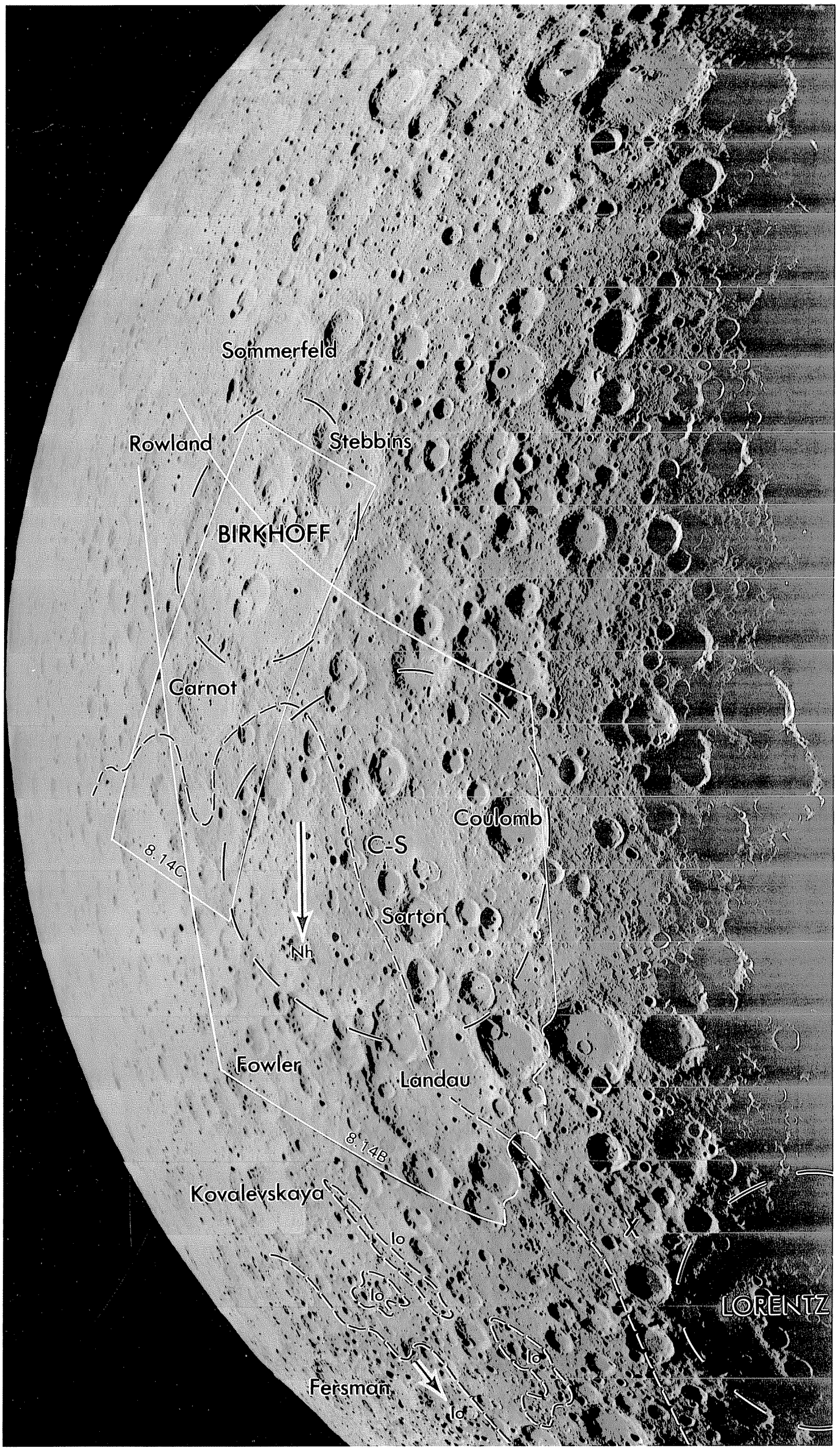
Sommerfeld
Rowland
Stebbins
BIRKHOFF
Carnot
Coulomb
C-S
8.14C
Sarton
Nh
Fowler
Landau
8.14B
Kovalevskaya
Io
Io
Io
Io
LORENTZ
Fersman

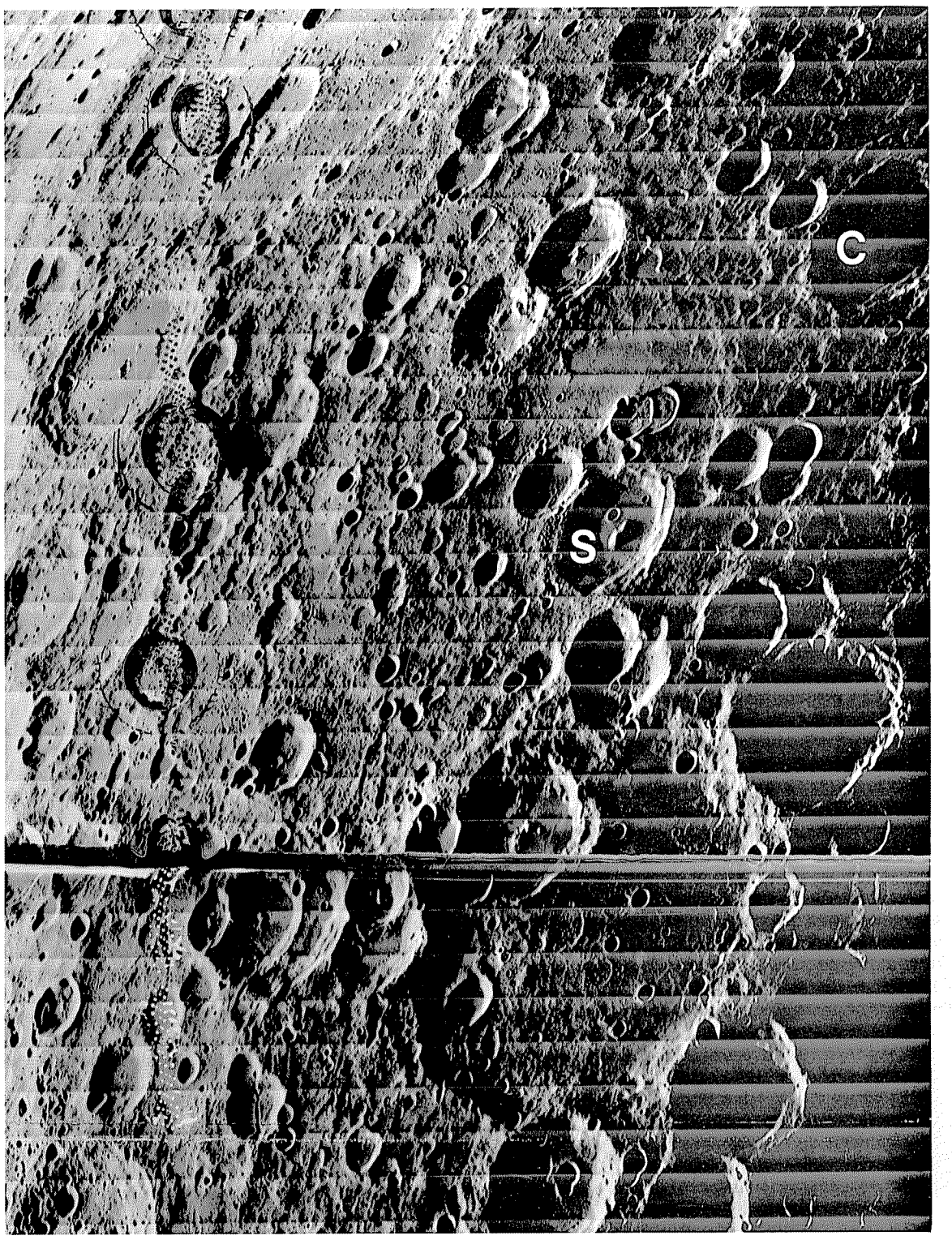

B. Detail of Coulomb-Sarton basin and superposed craters, including Coulomb (C) and Sarton (S). Orbiter 5 frame H–24.

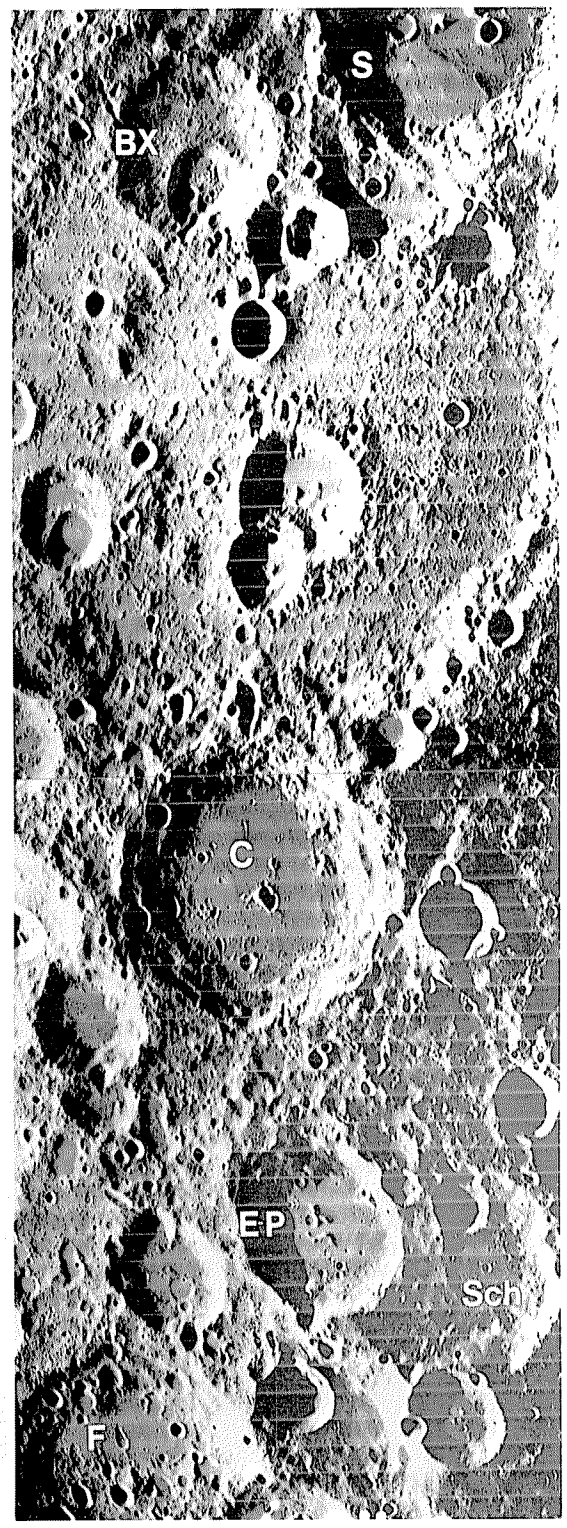

C. Craters superposed on Birkhoff include Stebbins (S; 135 km, 64.°5 N., 142.5° W.) and Birkhoff X (BX; 77 km, 62° N., 149.5° W.), probably pre-Nectarian; and Carnot (C; 52.5° N., 144° W.), fresher appearing than the others, probably Nectarian. Numerous pits on floor of Birkhoff are probably secondary craters of Stebbins, Carnot, and other large nearby craters. Birkhoff deposits or secondary craters overlie pre-Nectarian craters Fowler (F), Schlesinger (Sch; 97 km, 47.5° N., 138.5° W.), and probably Esnault-Pelterie (E-P; 79 km, 47.5° N., 141.5° W.); sharper rim of E-P suggests, alternatively, degradation only by Carnot deposits and superposition on Birkhoff deposits. Secondary craters of Orientale and (or) Hertzsprung basins are conspicuous in Fowler (compare *A*). Orbiter 5 frame H–29.

FIGURE 8.14.—Stratigraphic relations of pre-Nectarian basins Birkhoff (59° N., 145.5° W.), Coulomb-Sarton (530? km, 52° N., 123° W.), and Lorentz (360 km, 34.5° N., 97° W.) on northeastern farside.

A. Widely spaced dashes outline basin rims. Interior of Coulomb-Sarton basin (C-S) is pitted by small subequal subdued craters probably secondary to Birkhoff and Lorentz, and is overlain by radial chains secondary to Nectarian Hertzsprung basin (Nh), centered in direction of arrow 1,350 km south of crater Fowler (136 km, 43° N., 145° W., pre-Nectarian); dashed line encloses additional secondaries and other outer deposits of Hertzsprung. Craters superposed on C-S basin include Landau (221 km, 43° N, 119° W., pre-Nectarian), Coulomb (89 km, 54.5° N., 114.5° W., Nectarian), and Sarton (69 km, 49.5° N., 121° W., Nectarian). Overlap of old craters by Lorentz ejecta is visible at X. Sharp small craters in lower left near crater Fersman (143 km, 18° N., 125° W., pre-Nectarian) are secondary to the Imbrian Orientale basin (Io; centered in direction of arrow) and to Hertzsprung. Kovalevskaya (111 km) is probably Upper Imbrian. Orbiter 5 frame M–8.

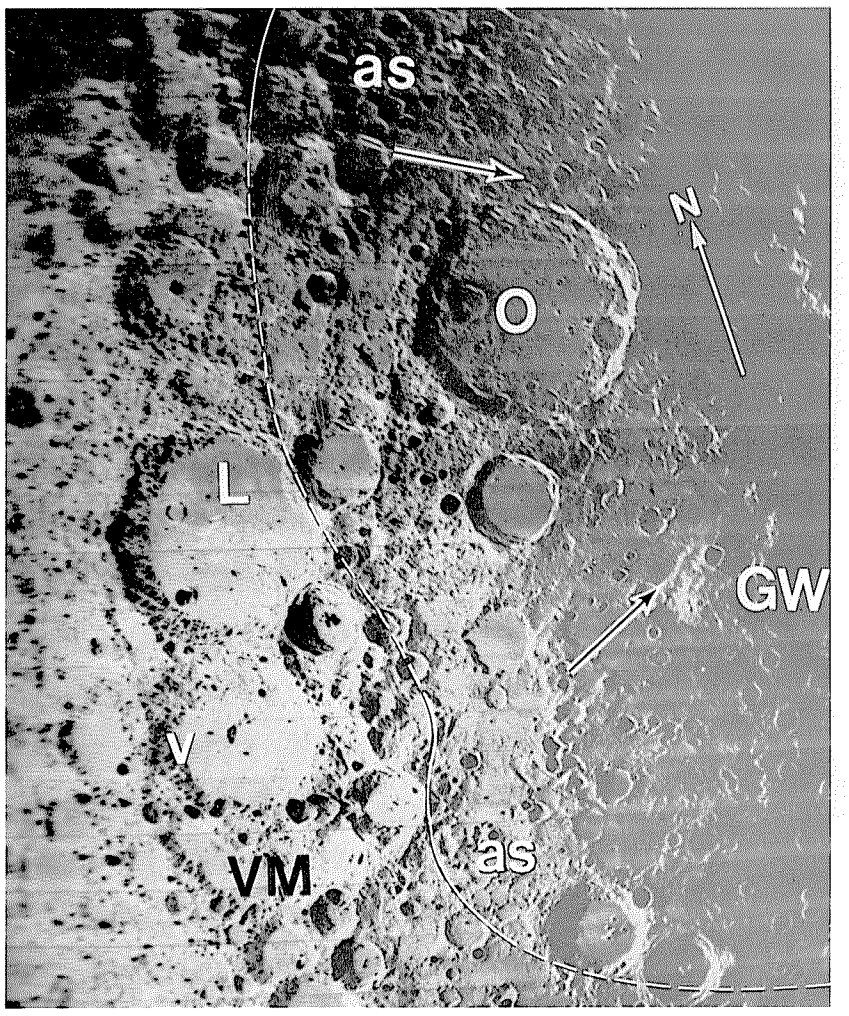

FIGURE 8.15.—Region west and southwest of Apollo basin, including Apollo-secondary craters (right of dashed line; most evident examples at letters as); black-and-white arrows point toward basin center. Center of indefinite basin Grissom-White (GW) is also indicated, but basin could be part of Apollo's peripheral structure. Pre-Nectarian craters include Leibnitz (L; 236 km), Von Kármán (V; 179 km, 44° S., 176° E.) and Von Kármán M (VM; 225 km). Oppenheimer (O; 206 km, 35° S., 166° W.) is believed to be Nectarian, though poorly photographed. Orbiter 5 frame M-43, rectified at University of Arizona's Lunar and Planetary Laboratory, Tucson, Ariz.

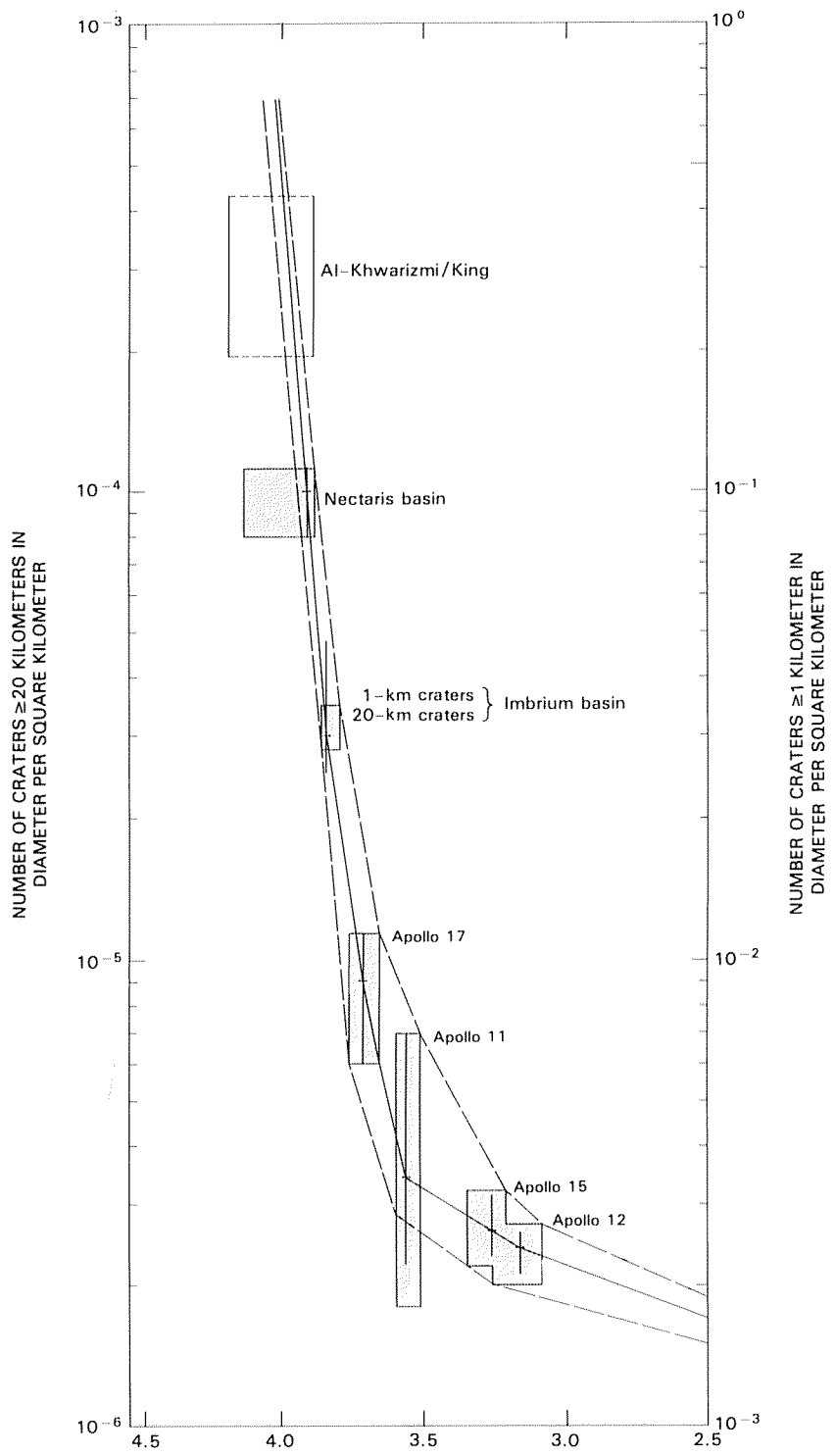

FIGURE 8.16.—Cratering rate during pre-Nectarian, Nectarian, and part of Imbrian time. Boxes represent observed crater densities (height) and absolute ages (width) given in later chapters; crosses represent my estimates for most likely values. Craters larger than 20 km in diameter (left vertical axis) were counted on Imbrium-basin and older units, and small craters (right vertical axis) on Imbrium-basin and younger units; Imbrium basin (fig. 10.4; table 7.3) provides calibration between cumulative frequencies of craters at 20- and 1-km diameters. Straight segments of curves drawn through corners of boxes enclose likely envelope of cratering frequencies as a function of time (dashed); heavy solid line is drawn through centers of crosses. Crater densities, but not absolute ages, are available for Al-Khwarizmi/King.